National School on Neutron and X-Ray Scattering

Argonne and Oak Ridge National Laboratories

Polarized Neutrons

20 August 2013

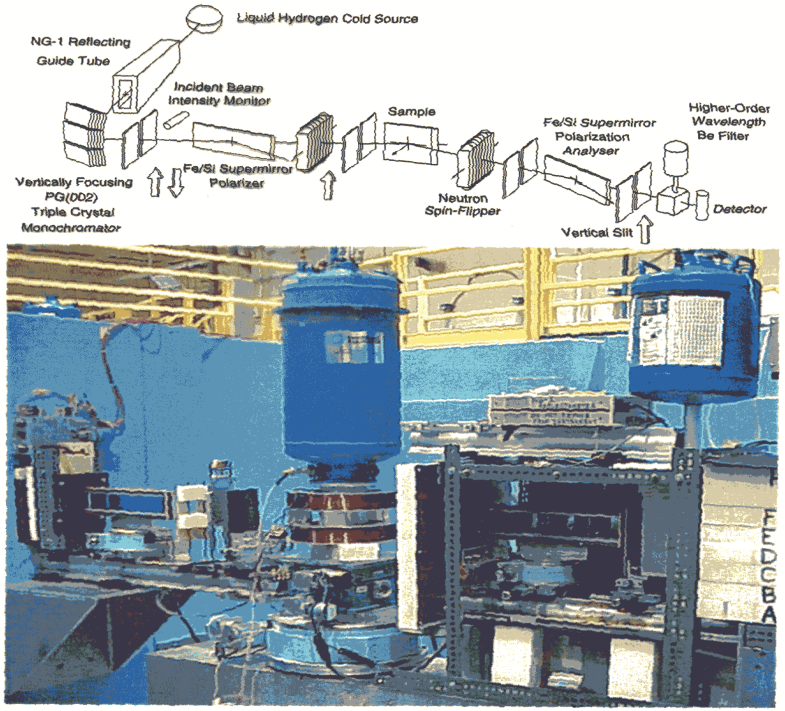

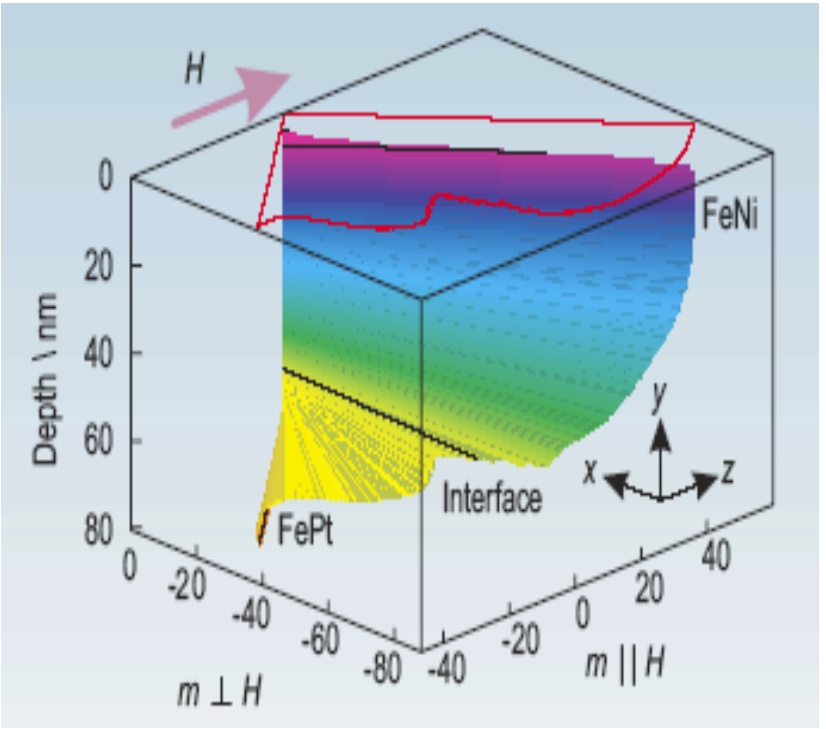

C.F.Majkrzak, *NIST Center for Neutron Research*,
Gaithersburg, MD

Part 1: Neutron Polarization

<> a magnetic moment arises from the motion of electrical charges -- though neutral, a neutron is composed of charged quarks which give rise to a net magnetic dipole moment which is quantized with corresponding spin 1/2 -- a neutron is a Fermion

<> if it exists at all, any neutron electric dipole moment is of negligible magnitude for all practical purposes of concern to us here

<> a neutron can be represented by a spinor wave function having two components corresponding to two spin eigen-states (spin “+” or “up” and “-” or “down”)

<> for a nucleus with spin, the neutron-nucleus (i.e., the *nuclear*) interaction is spin-dependent

<> the *magnetic* interaction between the neutron magnetic moment and that of a *nuclear* magnetic moment is relatively weak (and nuclear magnetic moments are normally not ordered -- a notable exception occurring in a 3He gas cell used as a neutron polarizer)

<> the *magnetic* interaction between the neutron magnetic moment and that of an atomic magnetic moment, on the other hand, can be comparable to the nuclear interaction

(a good description of the phenomenon of a quantized spin one-half system is given in the quantum mechanics text by Merzbacher)

$$\Psi = \psi_+ + \psi_- = \underbrace{C_{0+} e^{i\vec{k}_+ \cdot \vec{r}} \begin{pmatrix} 1 \\ 0 \end{pmatrix}}_{C_+} + \underbrace{C_{0-} e^{i\vec{k}_- \cdot \vec{r}} \begin{pmatrix} 0 \\ 1 \end{pmatrix}}_{C_-}$$

$$k_\pm = n_\pm k_0$$

$$n_\pm^2 = 1 - \frac{2m}{(\hbar k_0)^2}\left(V_N \pm \mu B\right)$$

$$= 1 - \frac{4\pi}{k_0^2}\left(\rho_N \pm \rho_M\right)$$

ρ_N: NUCLEAR SLD

ρ_M: MAGNETIC SLD

$$|\Psi|^2 = \Psi^{*T}\Psi = \begin{pmatrix} \psi_+^* & \psi_-^* \end{pmatrix}\begin{pmatrix} \psi_+ \\ \psi_- \end{pmatrix}$$

$$= \psi_+^* \psi_+ + \psi_-^* \psi_-$$

$$= C_{0+}^* e^{-i\vec{k}_+ \cdot \vec{r}} \, C_{0+} e^{+i\vec{k}_+ \cdot \vec{r}} + C_{0-}^* e^{-i\vec{k}_- \cdot \vec{r}} \, C_{0-} e^{+i\vec{k}_- \cdot \vec{r}}$$

$$= |C_{0+}|^2 + |C_{0-}|^2 = 1$$

GENERAL MULTILAYER REFLECTIVITY CALCULATION FOR POLARIZED NEUTRONS

$$\left[\frac{-\hbar^2}{2m}\nabla^2 + (V-E)\right]\Psi = 0 \qquad \Psi = \begin{pmatrix}\Psi_+ \\ \Psi_-\end{pmatrix}$$

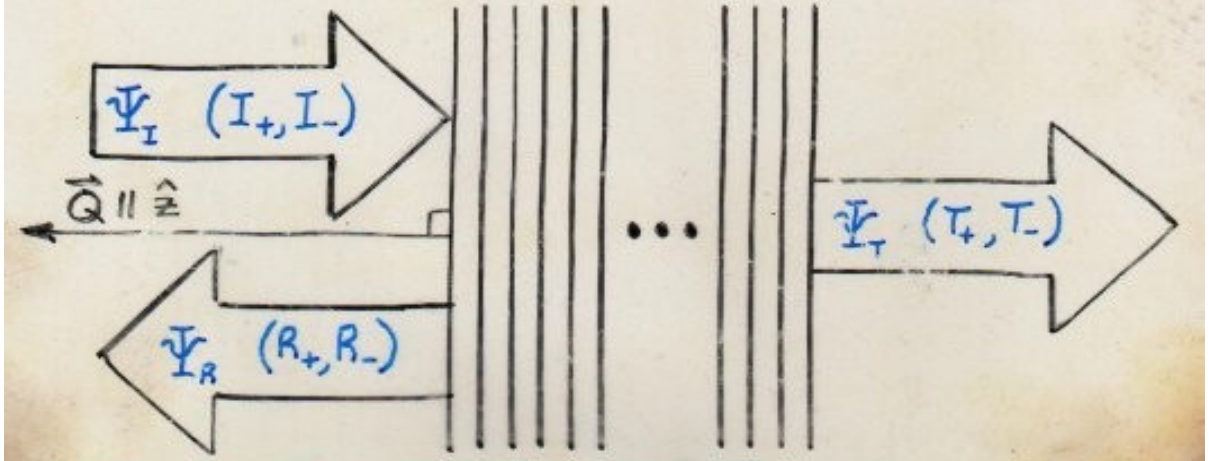

$$V_N = Nb$$

$$V_M = -\vec{\mu}\cdot\vec{B}$$

$$\frac{\partial^2}{\partial z^2}\Psi_+ + \left(\frac{Q^2}{4} - 4\pi\rho_{11}\right)\Psi_+ - 4\pi\rho_{12}\Psi_- = 0$$

$$\frac{\partial^2}{\partial z^2}\Psi_- + \left(\frac{Q^2}{4} - 4\pi\rho_{22}\right)\Psi_- - 4\pi\rho_{21}\Psi_+ = 0$$

$$\underset{(22)}{\rho_{11}} = Nb \underset{(-)}{+} Np\sin\theta\sin\phi$$

$$\underset{(21)}{\rho_{12}} = Np(\cos\theta \underset{(+)}{-} i\sin\theta\cos\phi)$$

$$\underline{V_M} = -\underline{\mu} \cdot \vec{B}$$

$$= -\gamma_m \left\{ \underline{S_x} B_x + \underline{S_y} B_y + \underline{S_z} B_z \right\}$$

$$= -\gamma_m \frac{\hbar}{2} \left\{ \begin{pmatrix} 0 & B_x \\ B_x & 0 \end{pmatrix} + \begin{pmatrix} 0 & -iB_y \\ iB_y & 0 \end{pmatrix} + \begin{pmatrix} B_z & 0 \\ 0 & -B_z \end{pmatrix} \right\}$$

$$= -\gamma_m \frac{\hbar}{2} \begin{pmatrix} B_z & B_x - iB_y \\ B_x + iB_y & -B_z \end{pmatrix}$$

$$= \frac{h^2}{2m\pi} \begin{pmatrix} N\rho_z & N\rho_x - iN\rho_y \\ N\rho_x + iN\rho_y & -N\rho_z \end{pmatrix}$$

- ONLY COMPONENTS OF $\vec{B} \perp \vec{Q}$ ARE EFFECTIVE IN SCATTERING NEUTRONS

$$\underline{\mu} = -\gamma_m \frac{\hbar}{2} \left\{ \begin{pmatrix} 0 & 1 \\ 1 & 0 \end{pmatrix} \hat{x} + \begin{pmatrix} 0 & -i \\ i & 0 \end{pmatrix} \hat{y} + \begin{pmatrix} 1 & 0 \\ 0 & -1 \end{pmatrix} \hat{z} \right\}$$

PIECEWISE CONTINUOUS SOLUTION :

$$\begin{pmatrix} T_+ \\ T_- \\ i\frac{Q}{2} T_+ \\ i\frac{Q}{2} T_- \end{pmatrix} = \hat{M}_T \begin{pmatrix} I_+ + R_+ \\ I_- + R_- \\ i\frac{Q}{2}[I_+ - R_+] \\ i\frac{Q}{2}[I_- - R_-] \end{pmatrix}$$

WHERE $|T_+|^2, |T_-|^2$ ARE THE TRANSMISSION PROBABILITIES

AND $|R_+|^2, |R_-|^2$ ARE THE REFLECTION PROBABILITIES

$$\hat{M}_T = \prod_{l=L}^{1} \hat{M}_l$$

($\hat{M}_l$ IS A 4X4 "TRANSFER" MATRIX CORRESPONDING TO THE l TH LAYER OF A MULTILAYER STRUCTURE)

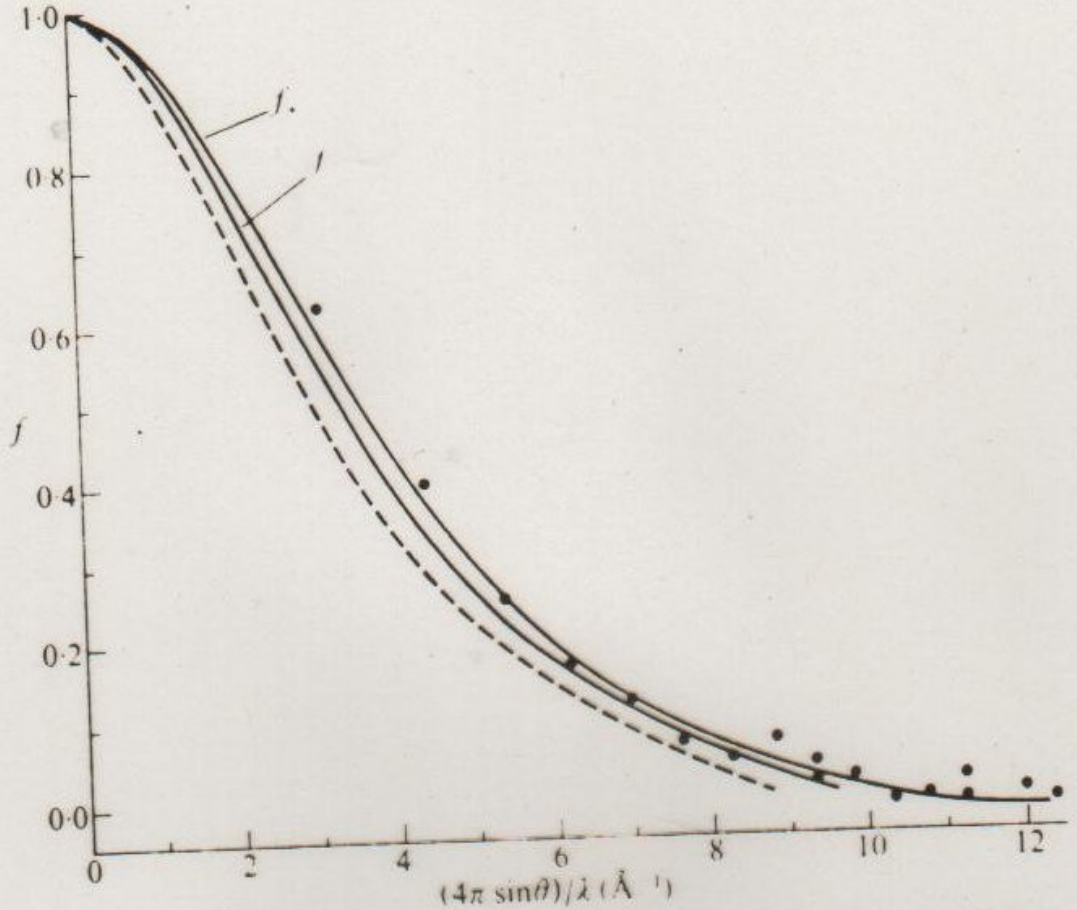

FIG. 126. Magnetic form factor curves for iron. The full-line curves show the calculation by Wood and Pratt for, respectively, the five 3d electrons of +ve spin and the single 3d electron of −ve spin for a free iron atom. The points are the experimental measurements of Shull and Yamada for metallic iron. The broken-line curve contrasts the experimental data for the Fe^{3+} ion in magnetite.

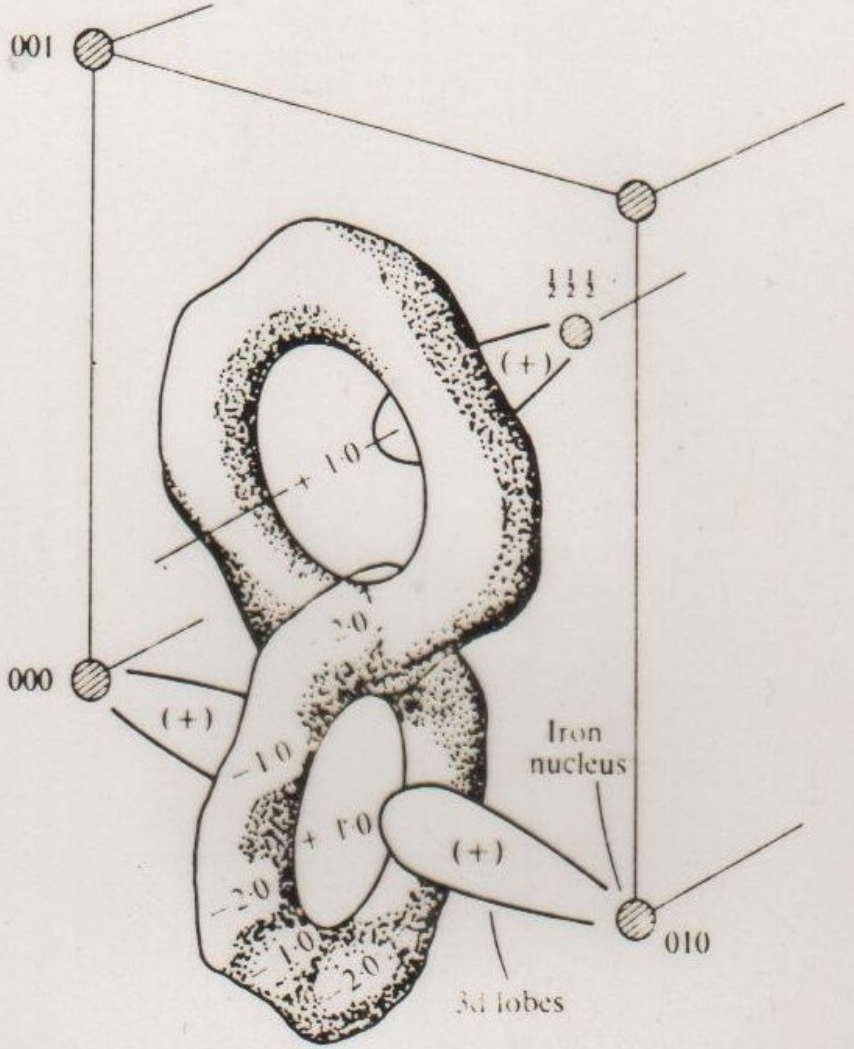

FIG. 134. The residual magnetization (kG) in iron as deduced experimentally by Shull and Mook (1966). The positive excess of 3d magnetization along the cube edges is over-emphasized in comparison with the interlocking rings of negative magnetization. The rings shown are centred on $0\frac{1}{2}0$, $0\frac{1}{2}\frac{1}{2}$.

Neutron Polarization Vector

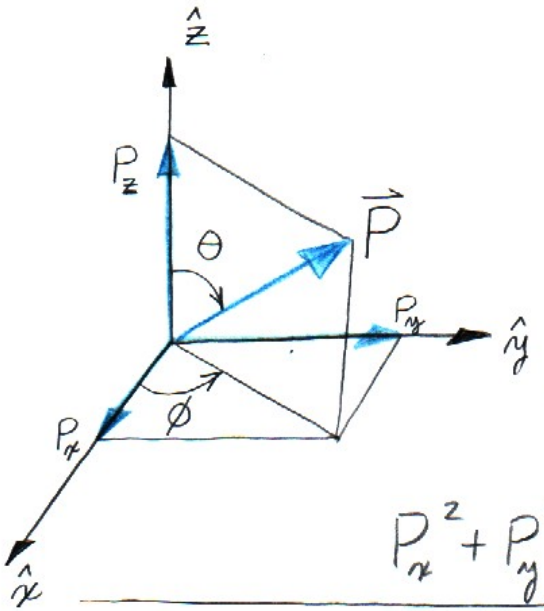

P_x	P_y	P_z	θ	ϕ	C_+	C_-
0	0	1	0	0	1	0
0	0	-1	π	0	0	1
1	0	0	$\pi/2$	0	$1/\sqrt{2}$	$1/\sqrt{2}$
0	1	0	$\pi/2$	$\pi/2$	$1/\sqrt{2}$	$i/\sqrt{2}$

$$\vec{P} = P_x \hat{x} + P_y \hat{y} + P_z \hat{z}$$

$$P_x^2 + P_y^2 + P_z^2 = 1$$

$$P_x = \sin\theta \cos\phi = 2\,\mathrm{Re}(C_+^* C_-)$$

$$P_y = \sin\theta \sin\phi = 2\,\mathrm{Im}(C_+^* C_-)$$

$$P_z = \cos\theta = |C_+|^2 - |C_-|^2$$

$$P_z = \frac{N_+ - N_-}{N_+ + N_-} \qquad |C_+|^2 = \frac{N_+}{N_+ + N_-} \qquad |C_-|^2 = \frac{N_-}{N_+ + N_-}$$

$$|C_+|^2 + |C_-|^2 = 1$$

$$C_+ = \cos\left(\frac{\theta}{2}\right)$$

$$C_- = \sin\left(\frac{\theta}{2}\right) e^{i\phi}$$

Polarization Rotation

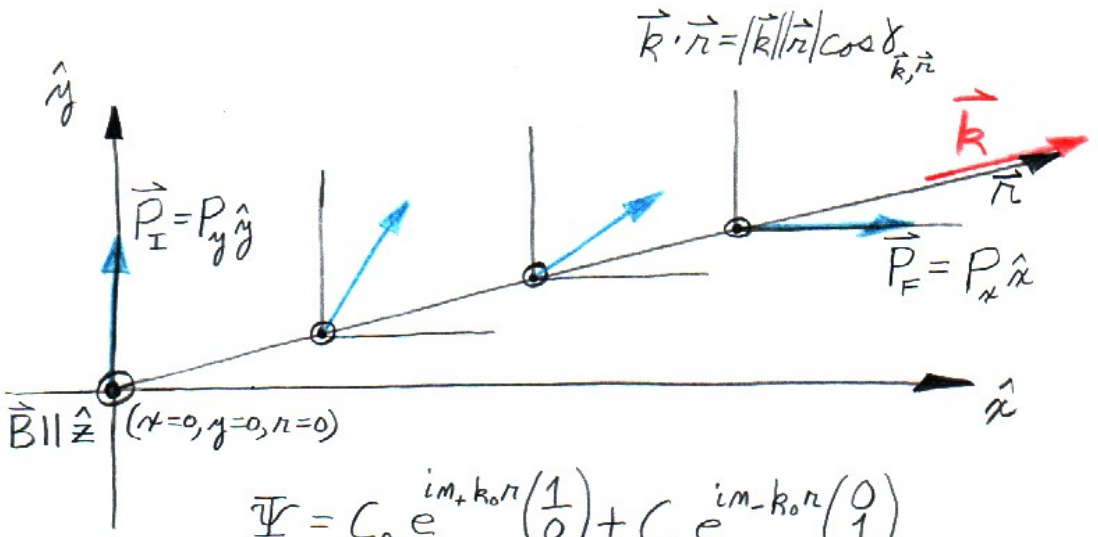

$$\Psi = \underbrace{C_{0+}e^{im_+k_0 r}}_{C_+}\begin{pmatrix}1\\0\end{pmatrix} + \underbrace{C_{0-}e^{im_-k_0 r}}_{C_-}\begin{pmatrix}0\\1\end{pmatrix}$$

$C_\pm = C_\pm(r)$ $\quad$ (at $r=0$, $C_\pm = C_{0\pm}$)

---

e.g. :

$$P_y(r) = 2\,\mathrm{Im}(C_+^* C_-)$$

$$= 2\,\mathrm{Im}\left[C_{0+}^* e^{-im_+k_0 r} C_{0-} e^{+im_-k_0 r}\right]$$

$$= 2\,\mathrm{Im}\left[\left(\tfrac{1}{\sqrt{2}}\right)\left(\tfrac{i}{\sqrt{2}}\right) e^{i(m_- - m_+)k_0 r}\right]$$

$$= \mathrm{Im}\left[i\cos\left([m_- - m_+]k_0 r\right) - \sin\left([m_- - m_+]k_0 r\right)\right]$$

$$\boxed{P_y(r) = \cos\left[(m_- - m_+)k_0 r\right]} \qquad (P_y(r=0) = 1)$$

Precession of the Polarization

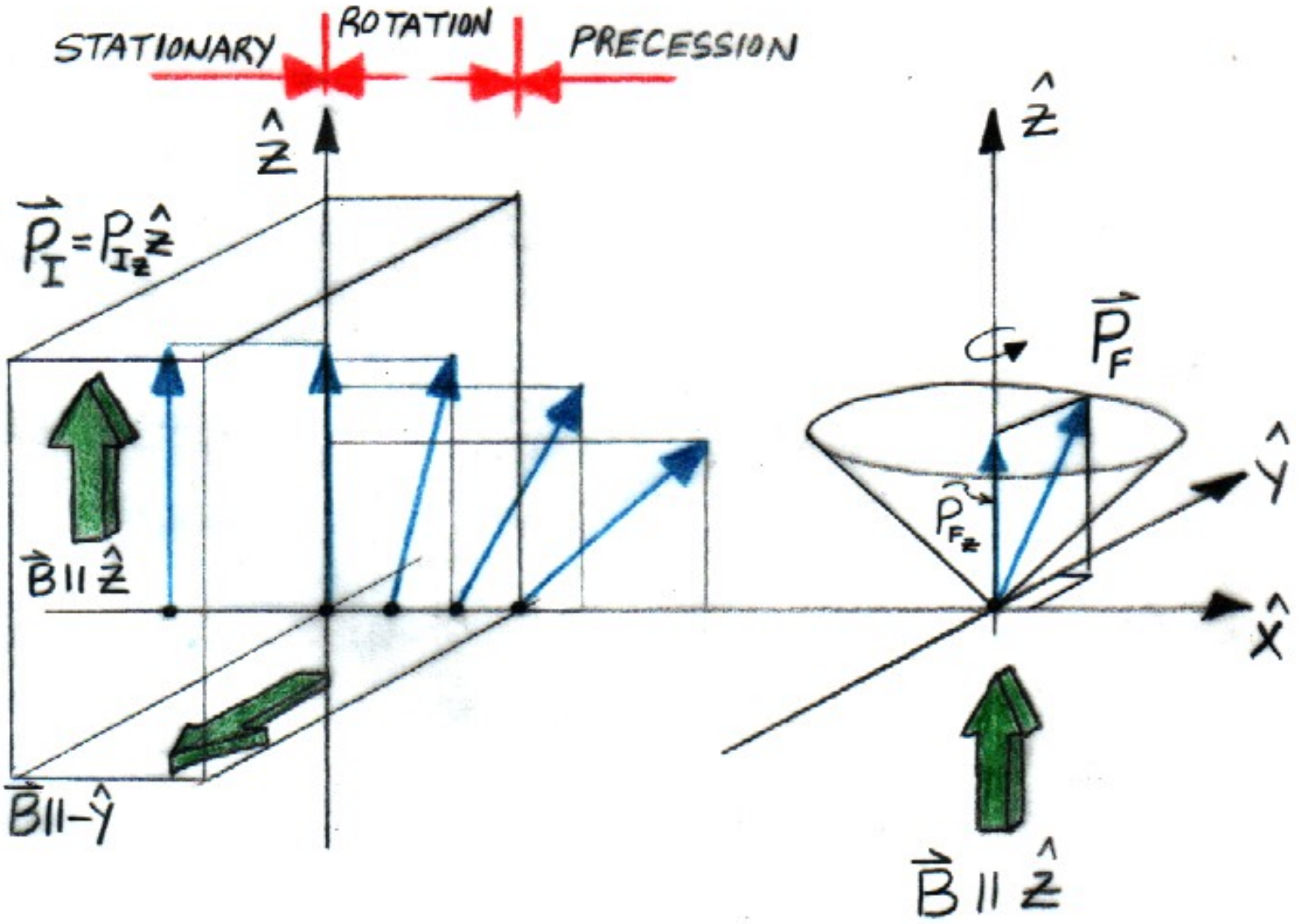

NEUTRON POLARIZER

By reflection from a magnetic film with nuclear and magnetic scattering length densities such that $\rho_N - \rho_M = 0$ (for "−" spin state) and $\rho_N + \rho_M \neq 0$ (for "+" spin state).

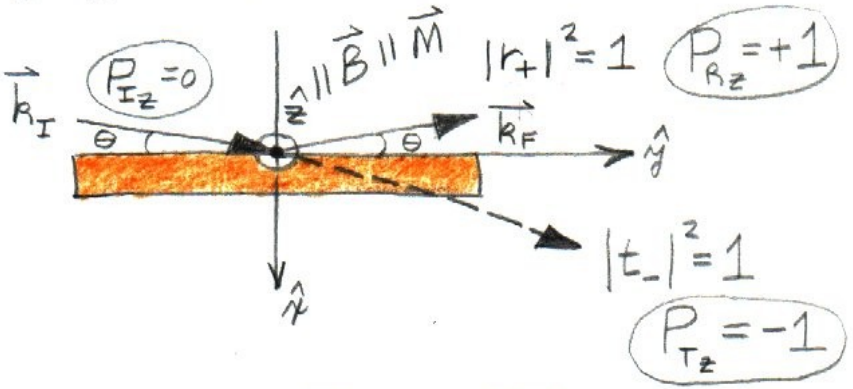

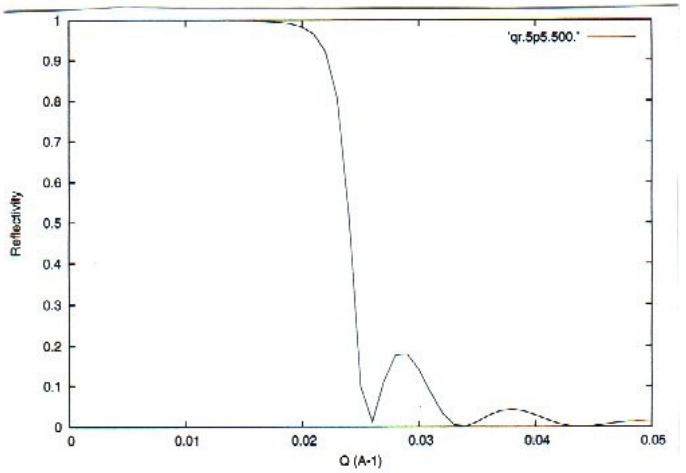

$|r_+|^2$

($|r_-|^2 = 0$, $|t_-|^2 = 1$)

(CALCULATED USING FORMULAS OF FIGURE 3)

$$Q = 2k_{0x} = 2k_0 \sin\theta$$

$$\rho_N + \rho_M = 10.0 \times 10^{-6}\ \text{Å}^{-2}$$

$$\rho_N - \rho_M = 0.0 \qquad L = 500.\ \text{Å}$$

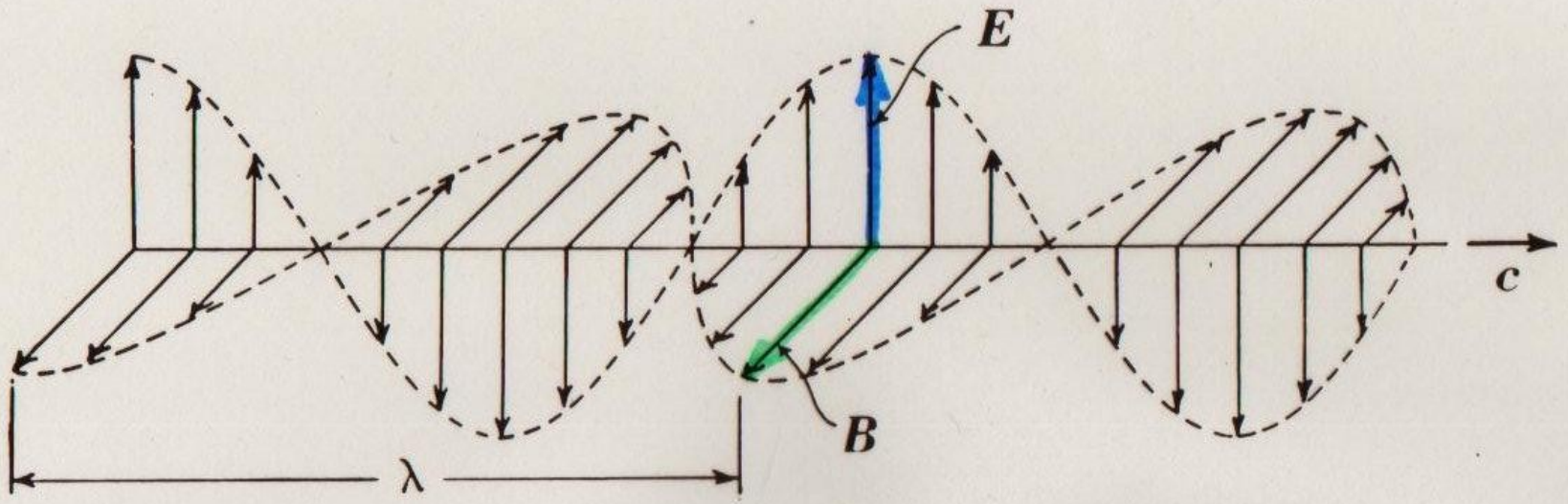

Figure 41-15. Representations of the electric and magnetic fields of a sinusoidal electromagnetic wave: (a) the field lines; (b) the sinusoidally varying amplitudes. (after Weidner & Sells, Elementary Classical Physics)

PHOTON

- ZERO MASS
- VELOCITY (IN VACUUM)

$$c_0 \cong 3 \times 10^8 \text{ m/sec}$$

- POLARIZED ELECTROMAGNETIC WAVE

Non-Resonant Magnetic X-Ray Scattering

<> X-rays interact with magnetic as well as with electronic charge distributions -- the magnetic scattering of x-rays is a relativistic effect.

<> For non-resonant x-ray scattering, $I_{MAGNETIC} / I_{CHARGE} \approx 10^{-6}$.

<> $r_{CHARGE} \alpha$ FT(charge density) x C

$r_{MAGNETIC} \alpha$ (1/2) FT(orbital density L) x A + FT(spin density S) x B

where the factors A, B, and C describe the polarization dependence of the scattering.

(For neutrons, the magnetic scattering amplitude is proportional to (L + 2S) so that the L and S contributions cannot be directly separated -- however, because the spatial extents of the magnetic densities corresponding to L and S are different, modeling and fitting allows for separation, at least in principle.)

Resonant Magnetic X-Ray Scattering

<> Resonant enhancement can be as large as 10^6.

<> Resonant magnetic scattering is element specific.

<> As an example, in Ho and at an incident x-ray energy near the L(III) absorption edge, the incident photon excites a 3p electron to the 5d unoccupied level -- under these conditions electric 2^L pole resonances are stimulated and contribute to the coherent scattering amplitude: the process can roughly be described as one in which a core electron is excited to an unoccupied level and forms a *magnetic resonance* with the *unpaired electrons* in that particular shell.

Details about magnetic x-ray scattering can be found, for instance, in the work of Doon Gibbs and colleagues on this subject (and from which the above information was obtained).

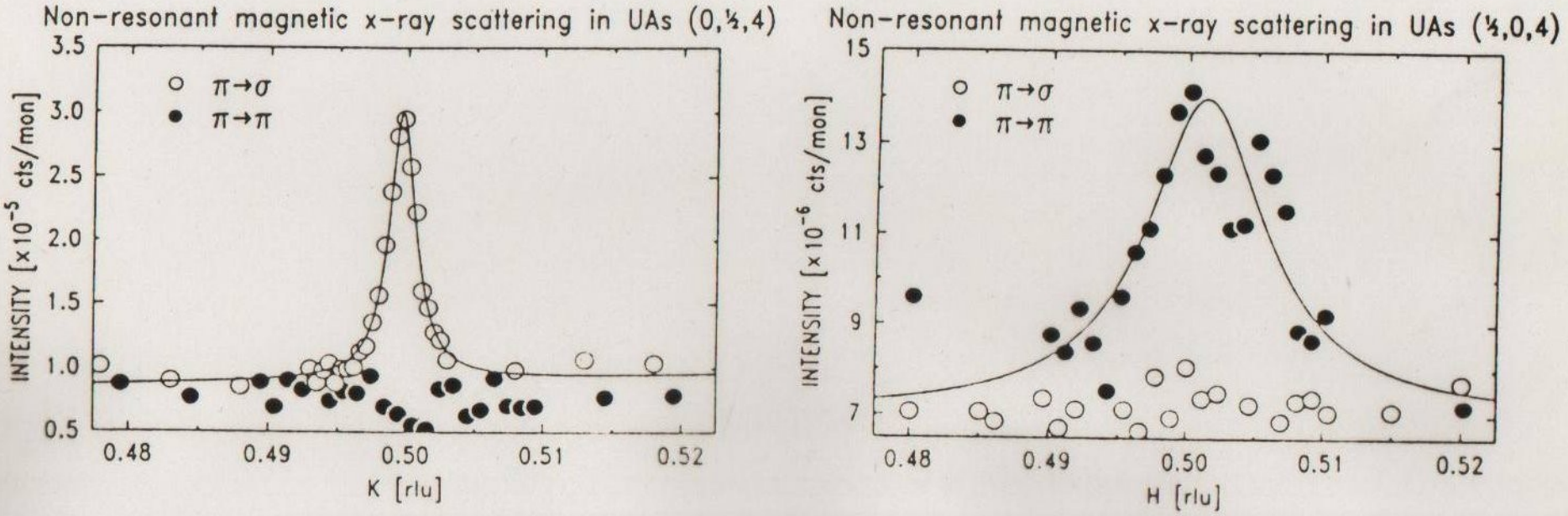

Fig. 2: Experimental results taken with different polarization (as indicated) for the satellites around the (004) charge peak in UAs. Based on Eq. (4) and our understanding of the magnetic structure (from neutrons) the structure factors are proportional to:

left hand side: $(\pi \rightarrow \pi)$ zero $(\pi \rightarrow \sigma)$ $(L + S)$

right hand side: $(\pi \rightarrow \pi)$ $(\sim 0.5L + S)$ $(\pi \rightarrow \sigma)$ $(\sim 0.1\ S)$

(AFTER G. LANDER et al.)

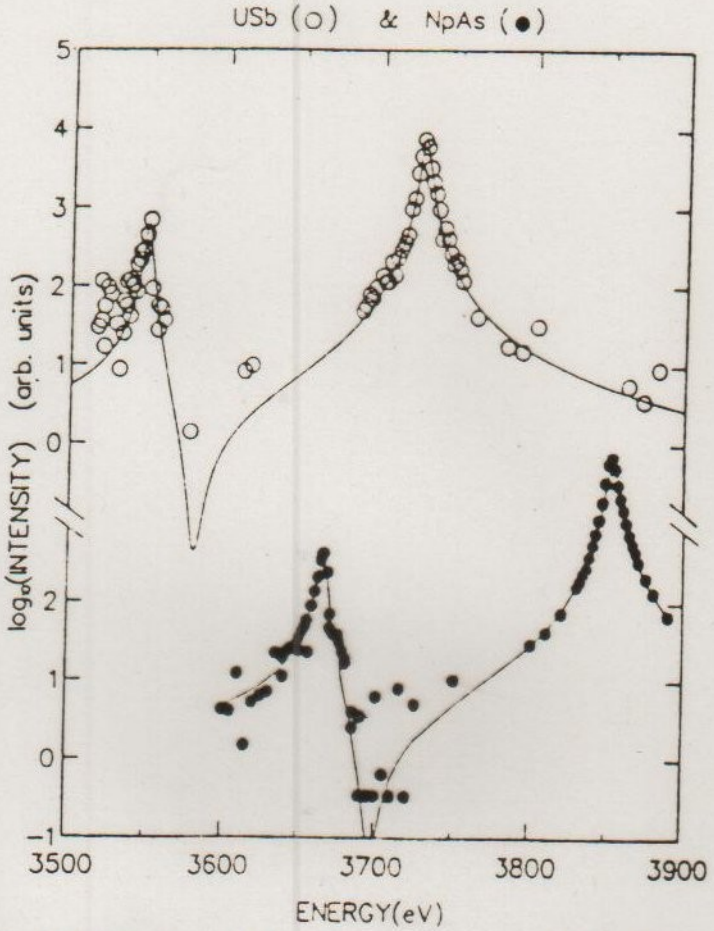

Fig. 3: Intensity of the magnetic satellite from a uranium and neptunium compound as a function of energy. The solid lines are fits to atomic resonance theory. (Taken from Ref. 24 and 25)

(D. GIBBS et al.)

(G. LANDER et al.)

Part 2: Application of Polarized Neutrons in Scattering Studies of Magnetic Condensed Matter

<> elastic scattering to determine magnetic *structures*

<> inelastic scattering to probe magnetic *excitations* such as spin waves

$$F^{\pm\pm} \propto \sum_{j=1}^{N} \left[b_{sj} \pm P_{sj} \cos\phi_j \right] e^{iQu_j}$$

$$F^{\pm\mp} \propto \sum_{j=1}^{N} P_{sj} \sin\phi_j \, e^{iQu_j}$$

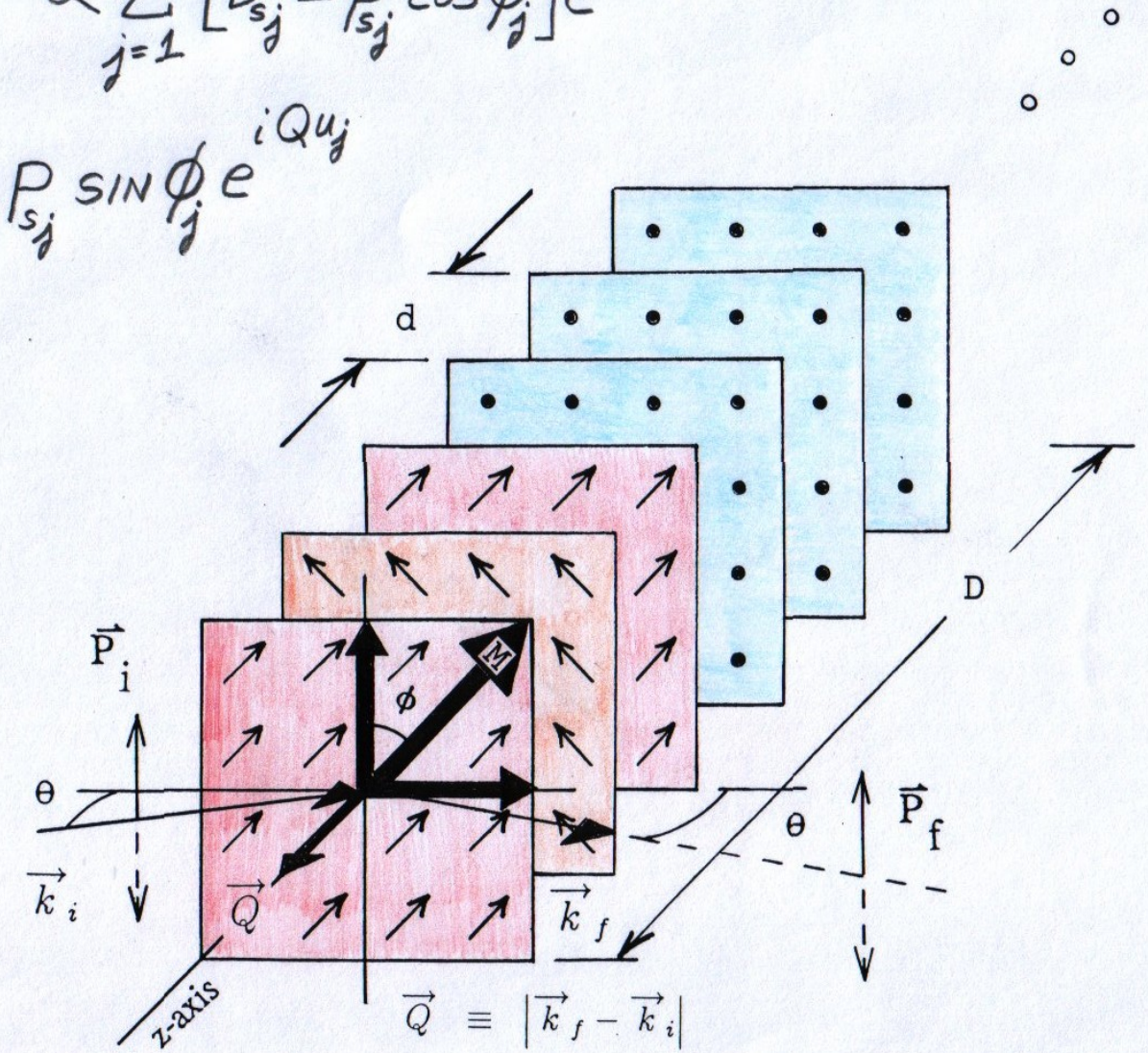

SELECTION RULES FOR SCATTERING OF POLARIZED NEUTRONS BY MAGNETIC MOMENTS

- ONLY MAGNETIZATION COMPONENTS $\perp \vec{Q}$ GIVE RISE TO SCATTERING
- COHERENT NUCLEAR SCATTERING : ALL NSF

- NUCLEAR SPIN INCOHERENT

FIELD AT SAMPLE	SF	NSF
$\vec{H} \parallel \vec{Q}$	2/3	1/3
$\vec{H} \perp \vec{Q}$	"	"

- ANTIFERROMAGNET OR PARAMAGNET

FIELD AT SAMPLE	SF	NSF
$\vec{H} \parallel \vec{Q}$	1	0
$\vec{H} \perp \vec{Q}$	1/2	1/2

- SPIRAL MAGNETIC STRUCTURES WITH SINGLE DOMAIN OF ONE CHIRALITY :

$\vec{H} \parallel \vec{Q}$ $\quad + \rightarrow -$ OR $- \rightarrow +$ SF ONLY,

DEPENDING ON WHETHER SPIRAL IS RIGHT- OR LEFT-HANDED

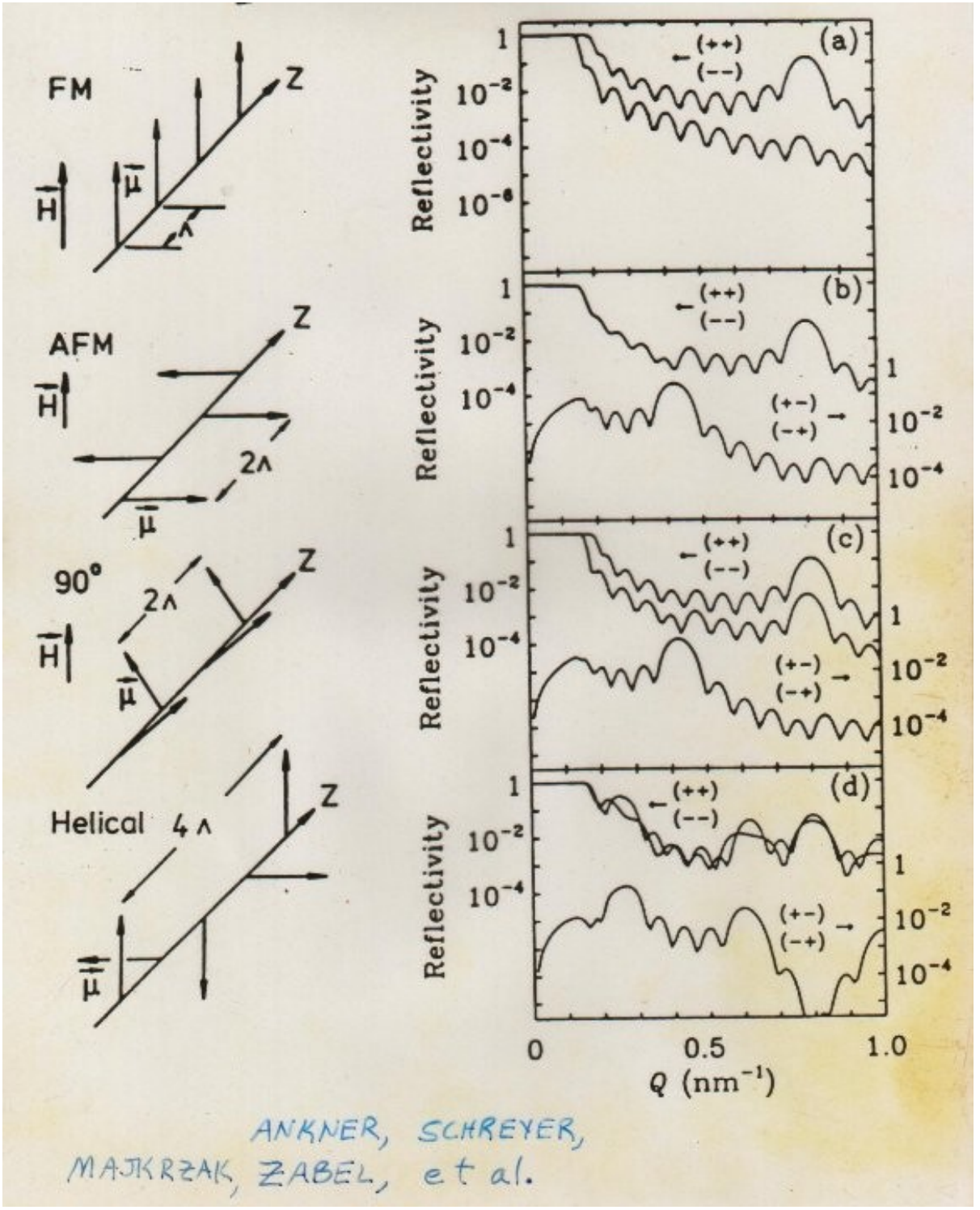

ANKNER, SCHREYER, MAJKRZAK, ZABEL, et al.

Polarized Beam Reflectometer (PBR) at NIST

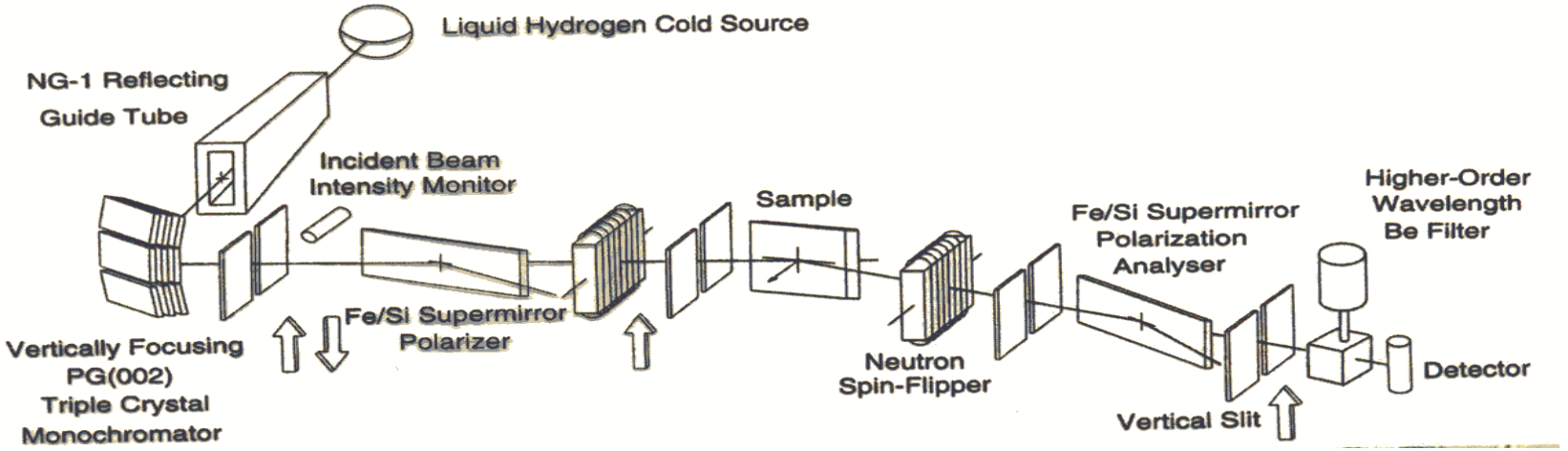

Epitaxial Growth of Superlattices

Magnetic Multilayers and Thin Films

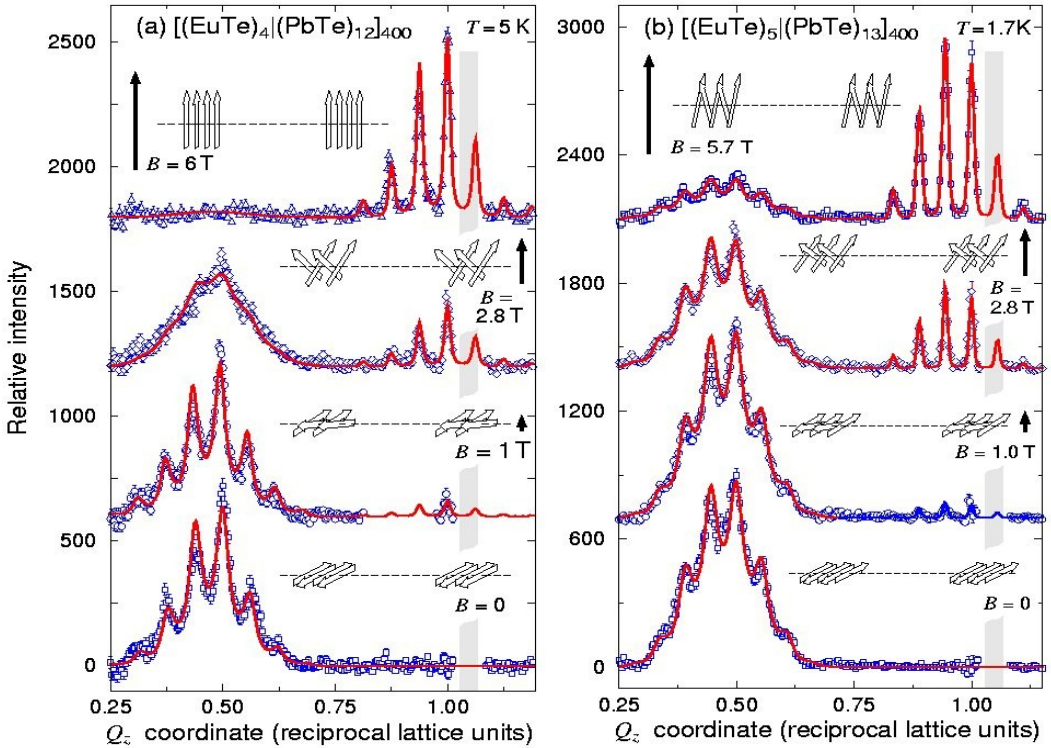

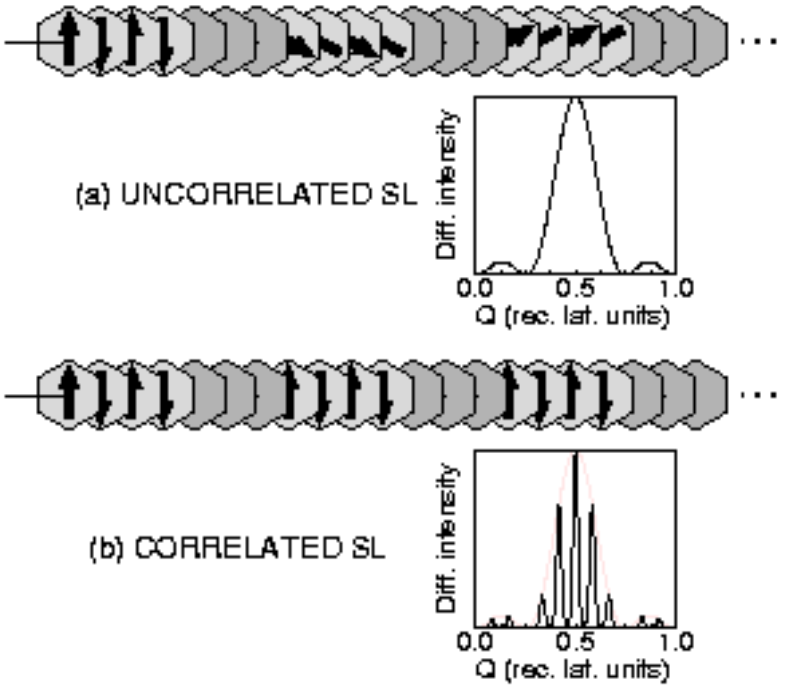

Polarized neutron reflection data on magnetic semiconductor superlattices by Henryk Kepa et al..

The Nobel Prize in Physics 2007

This year's Nobel Prize in Physics is awarded to ***ALBERT FERT*** *and* ***PETER GRÜNBERG*** *for their discovery of Giant Magnetoresistance. Applications of this phenomenon have revolutionized techniques for retrieving data from hard disks. The discovery also plays a major role in various magnetic sensors as well as for the development of a new generation of electronics. The use of Giant Magnetoresistance can be regarded as one of the first major applications of nanotechnology.*

Better read-out heads for pocket-size devices

Constantly diminishing electronics have become a matter of course in today's IT-world. The yearly addition to the market of ever more powerful and lighter computers is something we have all started to take for granted. In particular, hard disks have shrunk – the bulky box under your desk will soon be history when the same amount of data can just as easily be stored in a slender laptop. And with a music player in the pocket of each and everyone, few still stop to think about how many cds' worth of music its tiny hard disk can actually hold. Recently, the maximum storage capacity of hard disks for home use has soared to a terabyte (a thousand billion bytes).

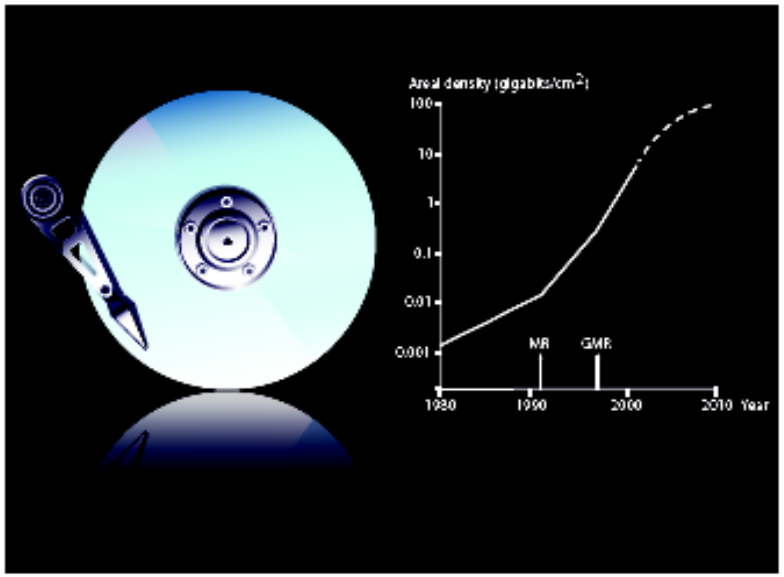

Diagrams showing the accelerating pace of miniaturization might give a false impression of simplicity – as if this development followed a law of nature. In actual fact, the ongoing IT-revolution depends on an intricate interplay between fundamental scientific progress and technical fine tuning. This is just what the Nobel Prize in Physics for the year 2007 is about.

9 October 2007

KUNGL. VETENSKAPSAKADEMIEN
THE ROYAL SWEDISH ACADEMY OF SCIENCES

Scientific Background on the Nobel Prize in Physics 2007

The Discovery of Giant Magnetoresistance

compiled by the Class for Physics of the Royal Swedish Academy of Sciences

The Royal Swedish Academy of Sciences, Information Department, Box 50005, SE-104 05 Stockholm, Sweden
Phone: +46 8 673 95 00, Fax: +46 8 15 56 70, E-mail: info@kva.se, Website: www.kva.se

As recounted in the “Scientific Background” material referred to on the left side of the page, prior to the discovery of the GMR effect by Gruenberg, polarized neutron diffraction studies of magnetic superlattices revealed an unambiguous coupling between magnetic layers across intervening nonmagnetic spacers. The interlayer coupling (IEC) observed in this neutron diffraction work was explained in terms of long-range exchange interactions, for example, the RKKY (Ruderman Kittel Kasuya Yosida) interaction. Interestingly, the underlying mechanism responsible for GMR was thus known about before the effect itself was discovered!

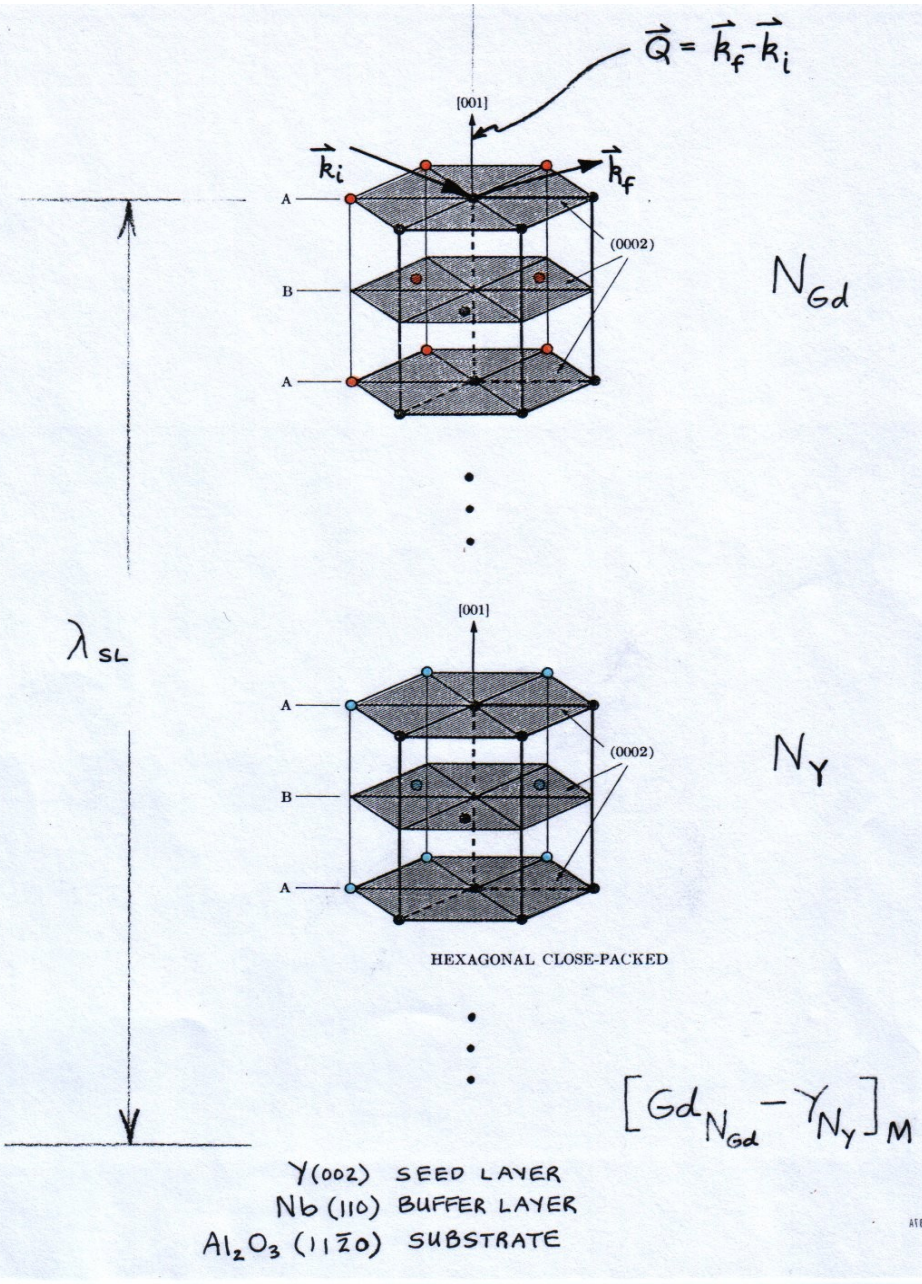
$\vec{Q} = \vec{k}_f - \vec{k}_i$
[001]
$\vec{k}_i$
$\vec{k}_f$
A
B
A
(0002)
N_{Gd}
λ_{SL}
[001]
A
B
A
(0002)
N_Y
HEXAGONAL CLOSE-PACKED
$[Gd_{N_{Gd}} - Y_{N_Y}]_M$
Y(002) SEED LAYER
Nb (110) BUFFER LAYER
Al_2O_3 $(11\bar{2}0)$ SUBSTRATE

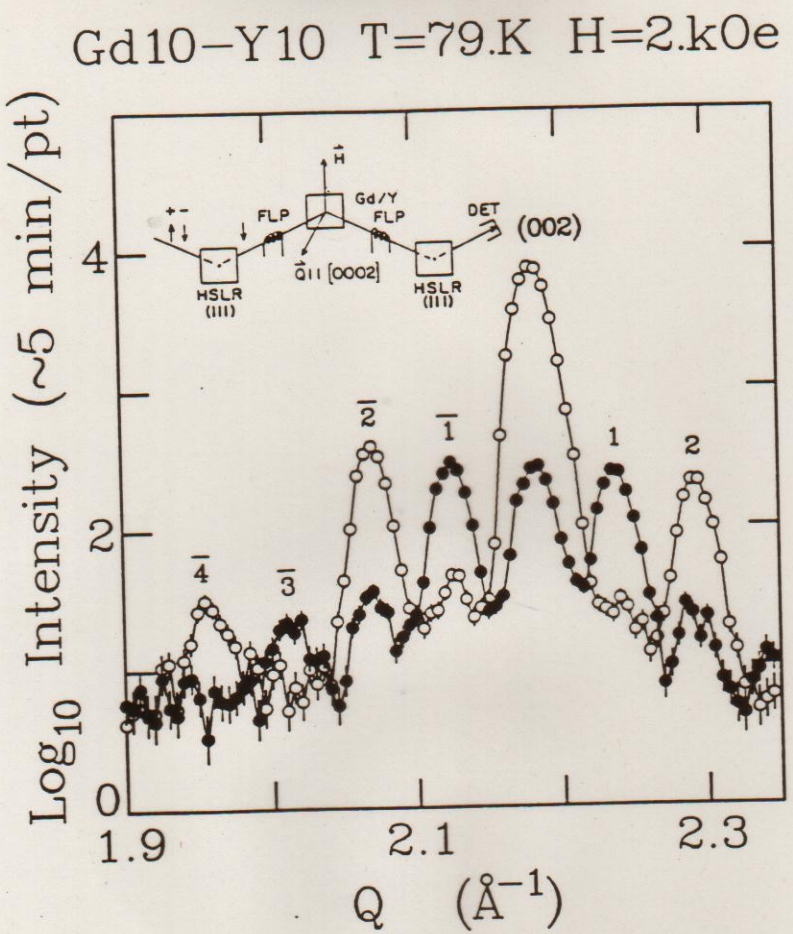

Fig. 7–1

Figure 7-1. NSF (open circles) and SF (filled circles) scattering from a [Gd_{10} - Y_{10}] superlattice as described in the text. The data have not been corrected for instrumental polarizing and flipping efficiencies (the SF scattering at the (002) position is predominantly, if not entirely, instrumental in origin). The SF scattering which appears at values of Q corresponding to a doubling of the chemical bilayer spacing (odd-numbered satellites) is consistent with an antiferromagnetic alignment (for an applied field approaching zero) of neighboring ferromagnetic Gd layers as depicted schematically in Figure 7-2. (After Majkrzak et al. (1986)).

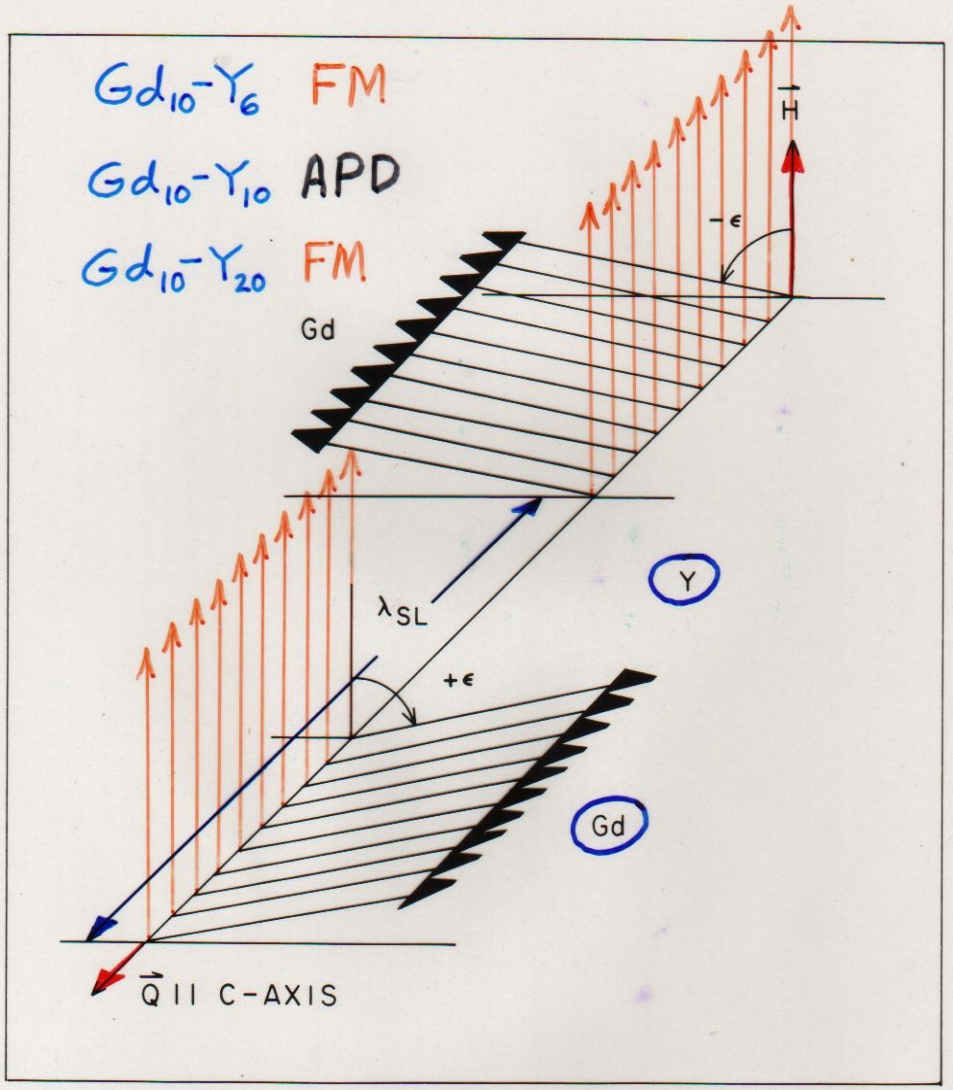
Gd_{10}-Y_6 FM
Gd_{10}-Y_{10} APD
Gd_{10}-Y_{20} FM
Gd
H
$-\epsilon$
λ_{SL}
$+\epsilon$
Y
Gd
$\vec{Q}$ II C-AXIS

• n-diffr. meas.

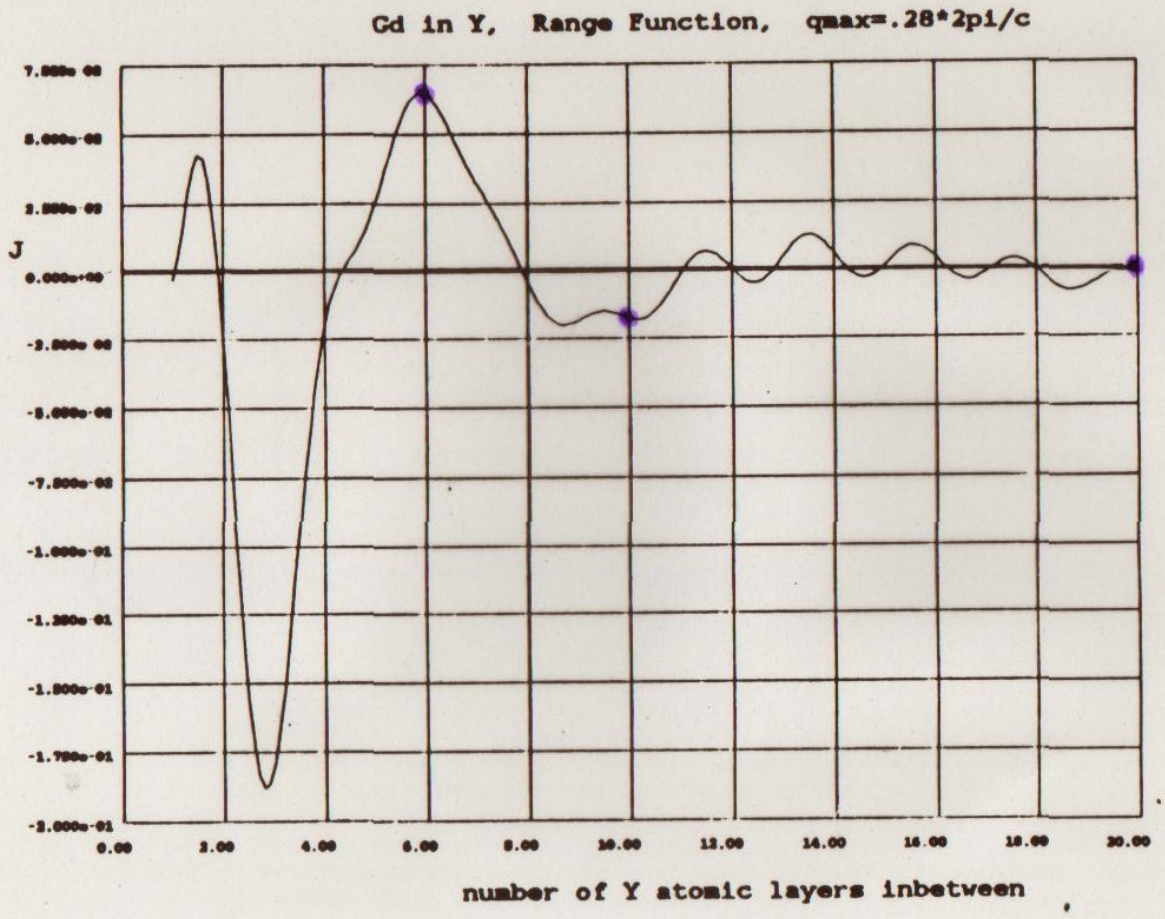
Gd in Y, Range Function, qmax=.28*2pi/c
J
0.00
2.00
4.00
6.00
8.00
10.00
12.00
14.00
16.00
18.00
20.00
number of Y atomic layers inbetween

TRANSVERSE AFM

FM SDW

Fe Cr

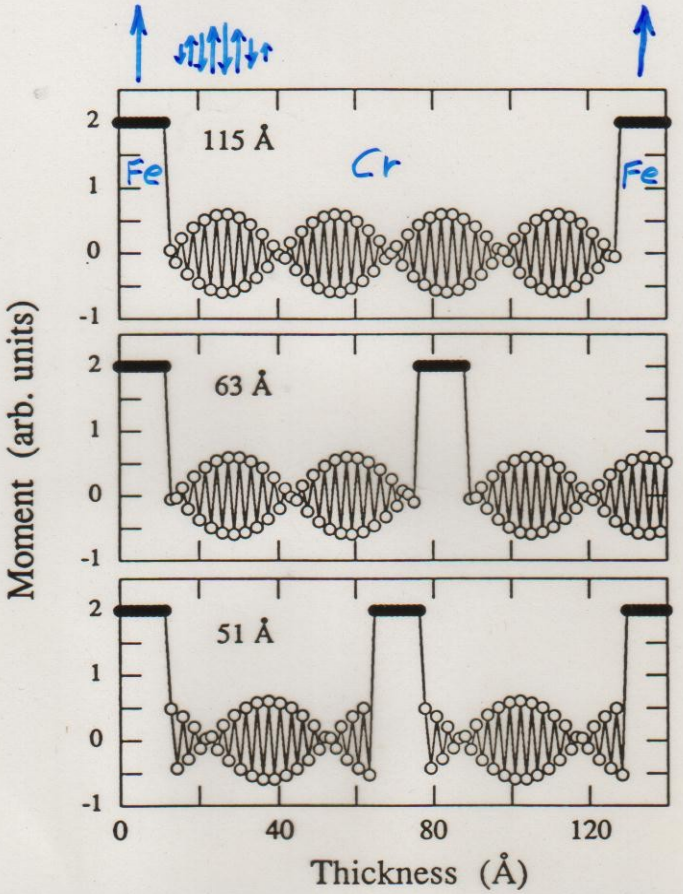

Fe/Cr SUPERLATTICES (GMR)

FULLERTON, BADER, & ROBERTSON

Figure 3

SCHREYER, ZEIDLER, ZABEL, ANKNER, MAJKRZAK, SCHÄFER, & GRÜNBERG, THIS CONFERENCE

NON COLLINEAR Fe/Cr (001)

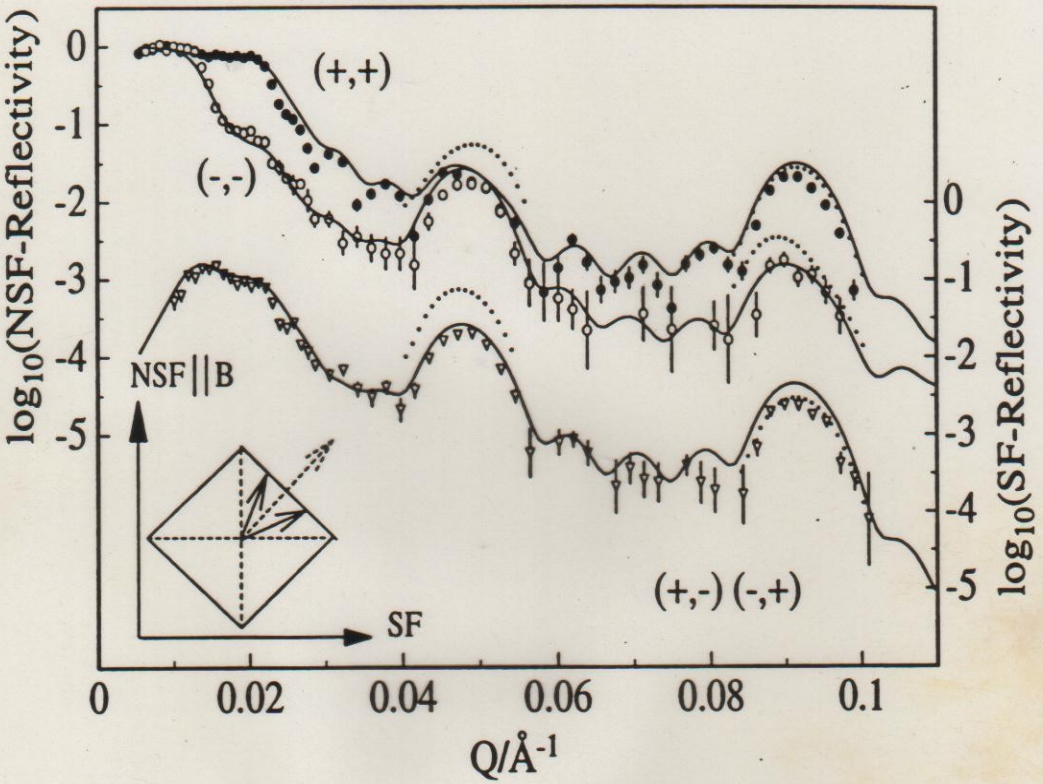

..... 90° ∢

— 50° ∢

$$E = -J_1 \frac{\vec{M}_1 \cdot \vec{M}_2}{|\vec{M}_1||\vec{M}_2|} - J_2 \left(\frac{\vec{M}_1 \cdot \vec{M}_2}{|\vec{M}_1||\vec{M}_2|} \right)^2$$

EXCHANGE COUPLING — BILINEAR — BIQUADRATIC

A. Schreyer etal.

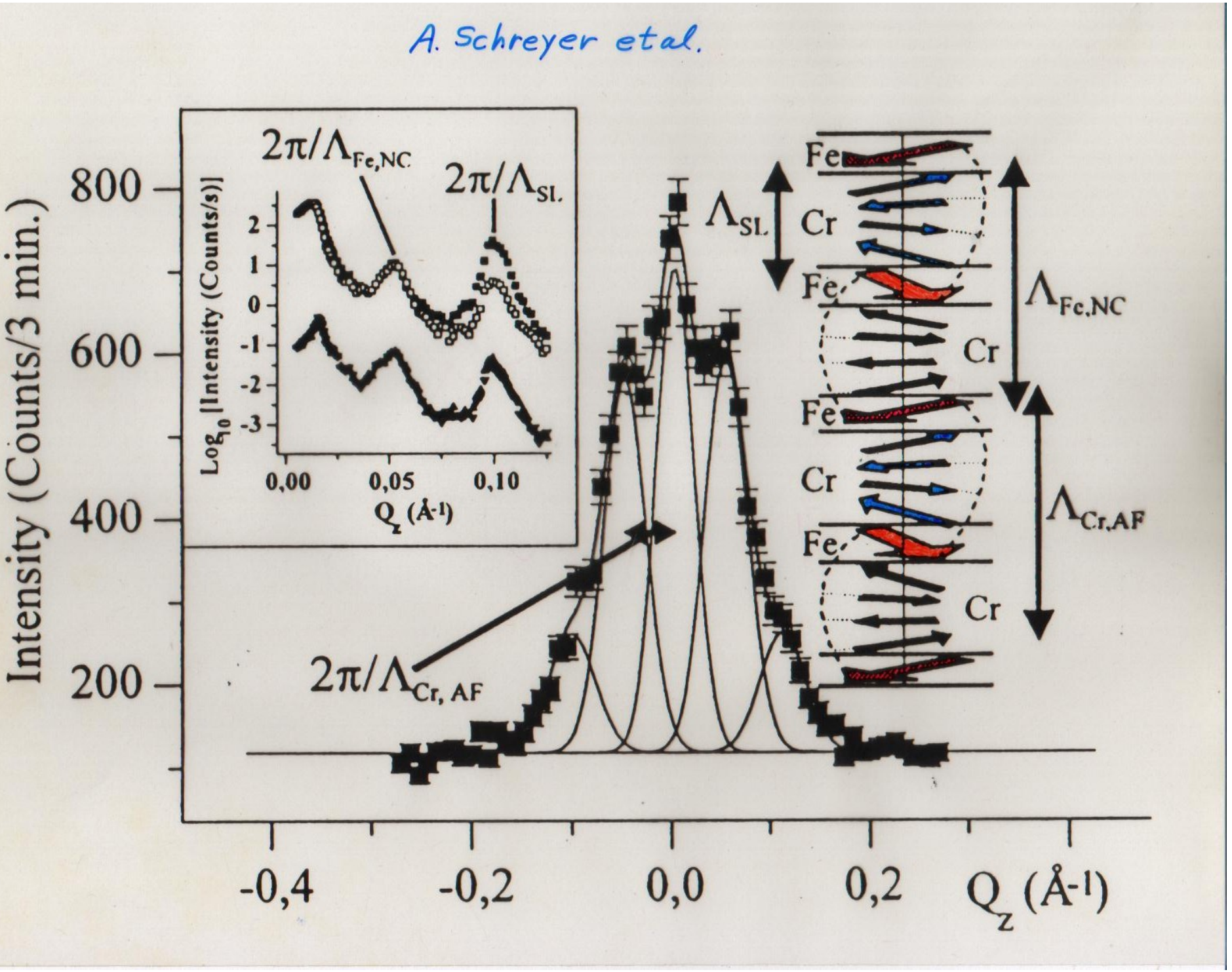

Magnetic Semiconductor Superlattices

Currently a great deal of attention is being focused on spintronics, a new area of solid-state electronics. In spintronics not only the electric current but also its spin state is controlled. Spin valves and spin injectors are the first practical applications of spintronics. Further progress in developing new devices hinges critically on the availability of suitable materials. Such materials need to be ?good? semiconductors, easy to integrate in typical integrated circuits, and their electronic properties should exhibit strong sensitivity to the carrier?s spin, ferromagnetism being an especially desirable property.

EuS is one of the very few natural ferromagnetic (F M) semiconductors. Since it becomes F M at a low temperature (T_c = 16.6 K) it is an unlikely choice for applications. However, studying the properties of heterostructures made on its base may give an important insight into fundamental processes taking place in all classes of materials under consideration.

GaMnAs is a man-made F M semiconductor. It is an example of a diluted magnetic semiconductor (D M S) in which a fraction of nonmagnetic cations (Ga) is substituted with magnetic ions (Mn). Such a material can readily be incorporated into modern GaAs-based semiconductor devices. Its T_c is still below room temperature, but this limitation may be lifted in other materials of this class (Refer to Reference 1).

Interlayer exchange coupling (I E C) in superlattices (S L), composed of ferromagnetic and nonmagnetic layers, is a crucial element of all spin-valve type devices that utilize the giant magnetoresistance effect. In metallic S L's currently being used, conduction electrons transfer the interlayer interactions through nonmagnetic spacers (Refer to Reference 2). Here we address the question whether I E C phenomena are possible in all-semiconductor superlattices, like EuS/PbS and GaMnAs/GaAs, where the carrier concentrations are many orders of magnitude lower than in metals.

The nonmagnetic spacer in EuS/PbS S L's is a narrow gap semiconductor with electron concentration of the order of 10^{17} cm^{-3} to 10^{18} cm^{-3}. For thin PbS layers (d_{PbS} < 70 Å) neutron reflectivity spectra, shown in Figure 1, have revealed a pronounced maximum of magnetic origin at the position corresponding to the doubled structural S L periodicity, thus indicating the existence of antiferromagnetic (A F M) interlayer arrangements (Refer to Reference 3).

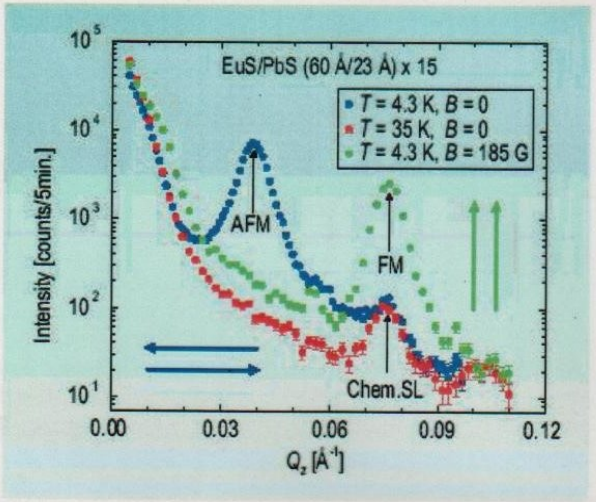

FIGURE 1. Unpolarized neutron reflectivity spectra for EuS/PbS S L with thin (23 Å) PbS spacer. Antiferromagnetic interlayer exchange coupling below T_c and at zero external field is clearly visible (blue curve). Applying a strong enough magnetic field (185 G in this case) parallel to the S L surface forces all the EuS layer?s magnetizations to ferromagnetic configuration (green curve). Above T_c the system is nonmagnetic, the only Bragg peak comes from the chemical S L periodicity.

For much thicker PbS spacers (d_{PbS} > 120 Å) the only magnetic peaks visible in the reflectivity profiles, see example in Figure 2, coincide with the chemical ones, thus leading to the conclusion that the magnetization vectors in adjacent EuS layers are parallel, which indicates F M I E C.

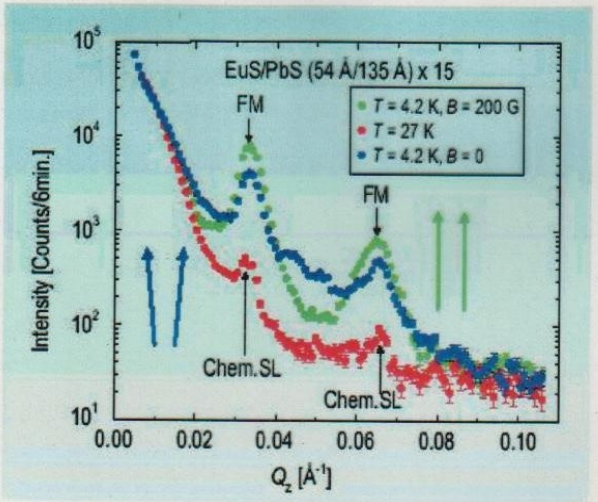

FIGURE 2. The sample with thick (135 Å) PbS layers is almost ferromagnetically coupled. Application of an external magnetic field enhances the F M Bragg peaks and lowers the intensity between them (at the A F M peak position).

In the intermediate PbS thickness range (70 Å < d_{PbS} < 120 Å), both A F M and F M peaks are present. Polarized neutron analysis of these maxima gives evidence that the magnetization vectors of adjacent EuS layers are not colinear. Hence, the I E C found in EuS/PbS S L's has an oscillatory character similar to that occurring in metallic S L's, although the oscillation period is much longer than the one in metallic systems.

In order to confirm that the free carriers, present in the PbS layer in such a small amount, are the cause of the observed oscillatory I E C, a series of analogous measurements have been carried out on EuS/YbSe S L's. The structure and lattice constant of YbSe are the same as those of PbS. In contrast to PbS, YbSe is a semi-insulator with a negligible carrier concentration. Neutron reflectivity profiles have shown no evidence of any interlayer coupling in the all investigated samples. That finding, together with the oscillatory character of coupling in S L's with PbS spacer, strongly points to the leading role of PbS free electrons in providing the necessary I E C mechanism, similar to that discovered in metallic multilayers.

Ferromagnetic ordering in GaMnAs is carrier (holes) induced; the Mn atoms, apart from being the magnetic element in the system, act also as acceptors providing the holes responsible for transferring exchange interactions between them. The details of the magnetic ordering, in particular its range, are still being disputed.

To address the latter issue, polarized neutron reflectometry has been performed on a number of GaMnAs/GaAs superlattices. Figure 3 shows an example of the obtained reflectivity profile in the vicinity of the first S L Bragg peak, for one of the samples. The very presence of the magnetic contribution to the structural S L Bragg peak is a strong confirmation of the F M I E C between consecutive GaMnAs layers. The absence of any spin-flip scattering shows that the sample is in a one-domain state, i.e., the F M ordering in GaMnAs is long range, and the sample is spontaneously saturated. The peak in (--) cross section, and its absence in the (++), is proof that the magnetization is directed oppositely to the external magnetic guide field, hence the long range ordering has formed spontaneously, without the influence of the external field. More details can be found in Reference 4.

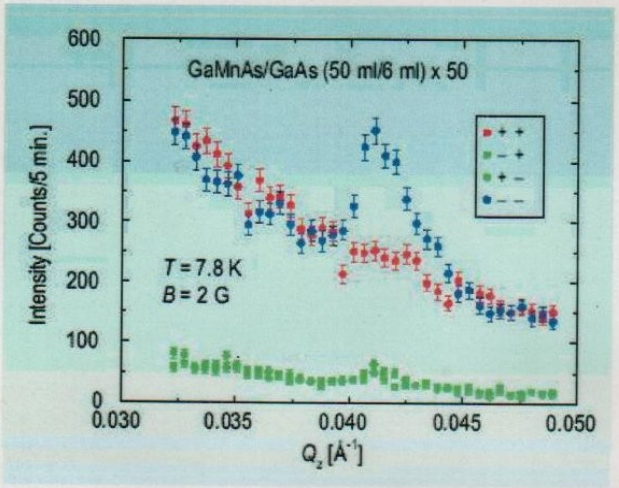

FIGURE 3. Polarized neutron reflectivity spectra for GaMnAs/GaAs superlattice.

References

[1] T. Dietl, H. Ohno, F. Matsukura, J. Cibert, D. Ferrand, Science 287,1018 (2000).

[2] P. Bruno, Phys. Rev. B52, 411 (1995).

[3] H. Kepa, J. Kutner-Pielaszek, J. Blinowski, A. Twardowski, C. F. Majkrzak, T. Story, P. Kacman, R. R. Galazka, K. Ha, H. J. M. Swagten, W. J. M de Jonge, A. Yu. Sipatov, V. Volobuev, T. M. Giebultowicz, Europhys. Lett. 56, 54 (2001).

[4] H. Kepa, J. Kutner-Pielaszek, A. Twardowski, C. F. Majkrzak, J. Sadowski, T. Story, T. M. Giebultowicz, Phys. Rev. B64, 121302 (2001).

Authors

A. Yu. Sipatov, V. Volobuev
Kharkov State Polytechnical University
Kharkov, Ukraine

H. Kepa, J. Kutner-Pielaszek, A. Twardowski
Institute of Experimental Physics
Warsaw University
Warsaw, Poland

T. Story, J. Sadowski
Institute of Physics
Polish Academy of Sciences
Warsaw, Poland

Pinpointing Chiral Structures with Front/Back Polarized Neutron Reflectometry

K. V. O'Donovan, J. A. Borchers, and C. F. Majkrzak
NIST Center for Neutron Research
National Institute of Standards and Technology
Gaithersburg, MD 20899-8562

O. Hellwig, E. E. Fullerton
IBM Almaden Research Facility
San Jose, CA 95120-6001

We have developed a new method of using polarized neutron reflectometry (PNR) to extract the structure of buried magnetic spirals in magnetic films. This technique improves upon earlier methods by being particularly sensitive to the presence of magnetic twists vis-à-vis structures in which the magnetization direction does not vary appreciably. Tracking the formation and growth of twists may solve a number of puzzles that hamper the development of magnetic thin film devices.

In collaboration with IBM scientists, we have applied the technique to a thin-film exchange-spring magnet and confirmed that the results may violate the current theory regarding the behavior of such magnets. It has been predicted that exchange-spring magnets, comprised of soft and hard ferromagnets in close proximity, are a composite that has a strong moment and does not readily demagnetize [1]. Therefore, exchange-spring magnets should give industry the ability to make much smaller permanent magnets for use in the magnetic recording devices, and elsewhere. As a side effect, when a small external magnetic field is opposed to that of the magnet, the portion of the soft ferromagnet farthest from the hard ferromagnet may twist into alignment with the field. When the field is removed, the soft ferromagnet untwists. The film provided by IBM consists of the hard ferromagnet $Fe_{55}Pt_{45}$ topped by the soft ferromagnet $Ni_{80}Fe_{20}$ [2].

Figure 1 shows a simplified diagram of the behavior predicted by current theories [1]. A magnetic field of 0.890 T, provided by an electromagnet, is sufficient to align both the soft and the hard layers of our exchange-spring magnet, as shown on the left. When a modest reverse field (on the order of 0.025 T) is applied to the exchange spring magnet, only the top of the soft layer will realign with the magnetic field. The hard layer remains pinned in the original direction, and a continuous twist is induced in the soft layer, as the direction of magnetization changes smoothly between the reverse field direction to the aligning field direction.

Although there are many alternatives to PNR to measure the magnetization, typically they measure only the average orientation of the magnetic spins, and cannot readily distinguish a spiral from a structure in which all the spins are canted with respect to an external field. PNR can extract the depth-dependence of the magnetic and chemical structure. We have studied the sample over a wide range of external magnetic fields, and can track the development of the spiral with field [3].

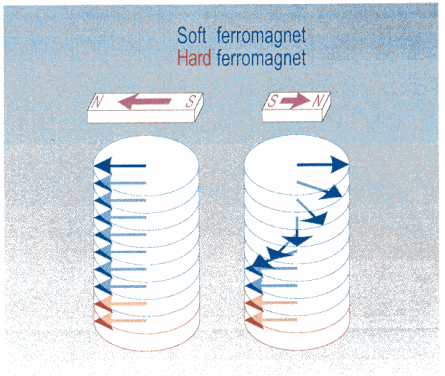

FIGURE 1. Model for field behavior of exchange-spring magnets. On the left the magnet has been aligned by a large external magnetic field. On the right a smaller field opposed to the first field causes a twist to form in the soft ferromagnet, while the hard ferromagnet remains aligned.

A PNR experiment begins with neutrons whose magnetic moments are aligned parallel (+) or opposite (–) to the external magnetic field. When the magnetization of the sample is perpendicular to this magnetic field, the neutron moment precesses as it interacts with the sample. When this happens the spin-flip (SF) reflectivities R^{+-} and R^{-+} are strong. If the magnetization of the sample is parallel to the external magnetic field, no precession occurs, but the non-spin-flip (NSF) reflectivities R^{++} and R^{--} will differ. The NSF reflectivities also provide information about the chemical structure of the film.

Our new modification of the PNR method greatly enhances the contrast between colinear and certain non-colinear magnetic structures [4]. We first measure the reflectivity with neutrons glancing off the front surface of the material, and then repeat with neutrons glancing off the back surface. The experiment is akin to holding the plane of the film up to a "magnetic mirror" to see whether the mirror image is the same as the original structure. In a colinear structure, all the spins are aligned along a common direction, and the mirror image is very much like the original structure.

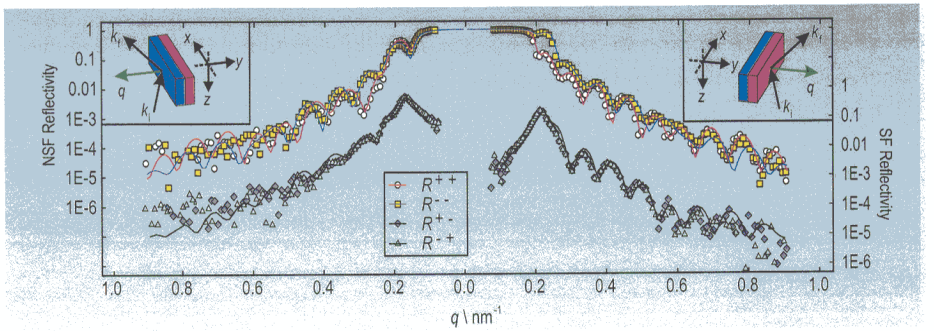

FIGURE 2. Reflectivity of a $Ni_{80}Fe_{20}|Fe_{55}Pt_{45}$ bilayer. The front reflectivity is plotted on the right while the back reflectivity is plotted on the left. The SF reflectivities R^{+-} and R^{-+} are plotted against the right ordinate axis. The NSF reflectivities R^{++} and R^{--} are plotted against the left ordinate axis.

But the mirror image of a magnetic twist to the right is a magnetic twist to the left. Therefore, if the front and back reflectivities are significantly different, we can deduce the presence of a spiral. Fitting the data confirms the spiral's existence.

Figure 2 shows data collected at 0.026 T after aligning in -0.89 T. Fits to the data are shown as solid lines. The data from the front reflectivity are shown on the right, and the data from the back reflectivity are shown on the left. The spin-flip (SF) reflectivities R^{+-} and R^{-+} are plotted against the right-hand axis, which have been shifted relative to the NSF reflectivities R^{++} and R^{--} plotted against the left axis. At $q = 0.2$ nm^{-1}, there is a splitting in the front NSF reflectivity that is much more pronounced than that of the back reflectivity at the same q. This is a hallmark of the spiral structure.

Figure 3 shows the magnetic structure that gives the excellent fit to the data plotted in Fig. 2. The location of the hard/soft interface is marked in Fig. 3. Surprisingly, we discover the spiral invades the hard ferromagnet even at extremely low fields. Current theory predicts that when this occurs, the soft ferromagnet will not be able to untwist fully. Yet, other magnetic studies show that our exchange-spring magnet does untwist when this field is removed. Thus, our PNR measurements have identified a shortcoming of current theory.

With this new technique, NIST is now able to better characterize the magnetic properties of thin films, which can improve the capability and reliability of industrial devices for magnetic recording and sensing.

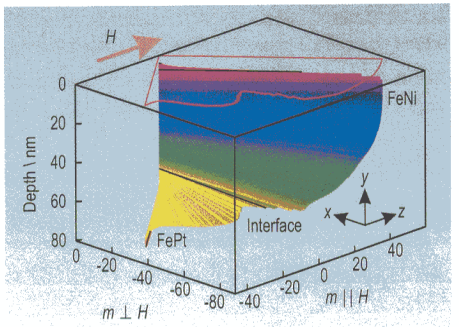

FIGURE 3. Fitted magnetization of the data presented in Fig. 2. The front of the sample is at a depth of 0 nm and the back is at a depth of 70 nm. The red curve is a projection of the magnetic structure into the plane of the front surface.

References

[1] E. F. Kneller and R. Hawig, IEEE Trans. Magn. **27**, 3588 (1991).

[2] O. Hellwig, J. B. Kortright, K. Takano, and E. E. Fullerton, Phys. Rev. **B62**, 11694 (2000).

[3] K. V. O'Donovan, *et al.*, in preparation.

[4] K. V. O'Donovan, *et al.*, submitted to Applied Physics A.

Part 3: Application of Polarized Neutrons to Measurements of Very Small Energy and Momentum Transfers with Condensed Matter Systems

<> the precession of the neutron spin in a magnetic field can be used as an accurate measure of length from which changes in angle (momentum or wavevector direction) or neutron speed (energy or wavevector magnitude) can be determined

Neutron spin-echo labeling of angle: after work of Felcher, te Velthuis, Rekveldt, Pynn, Major and others. (Thanks to Suzanne te Velthuis for this and next figure!)

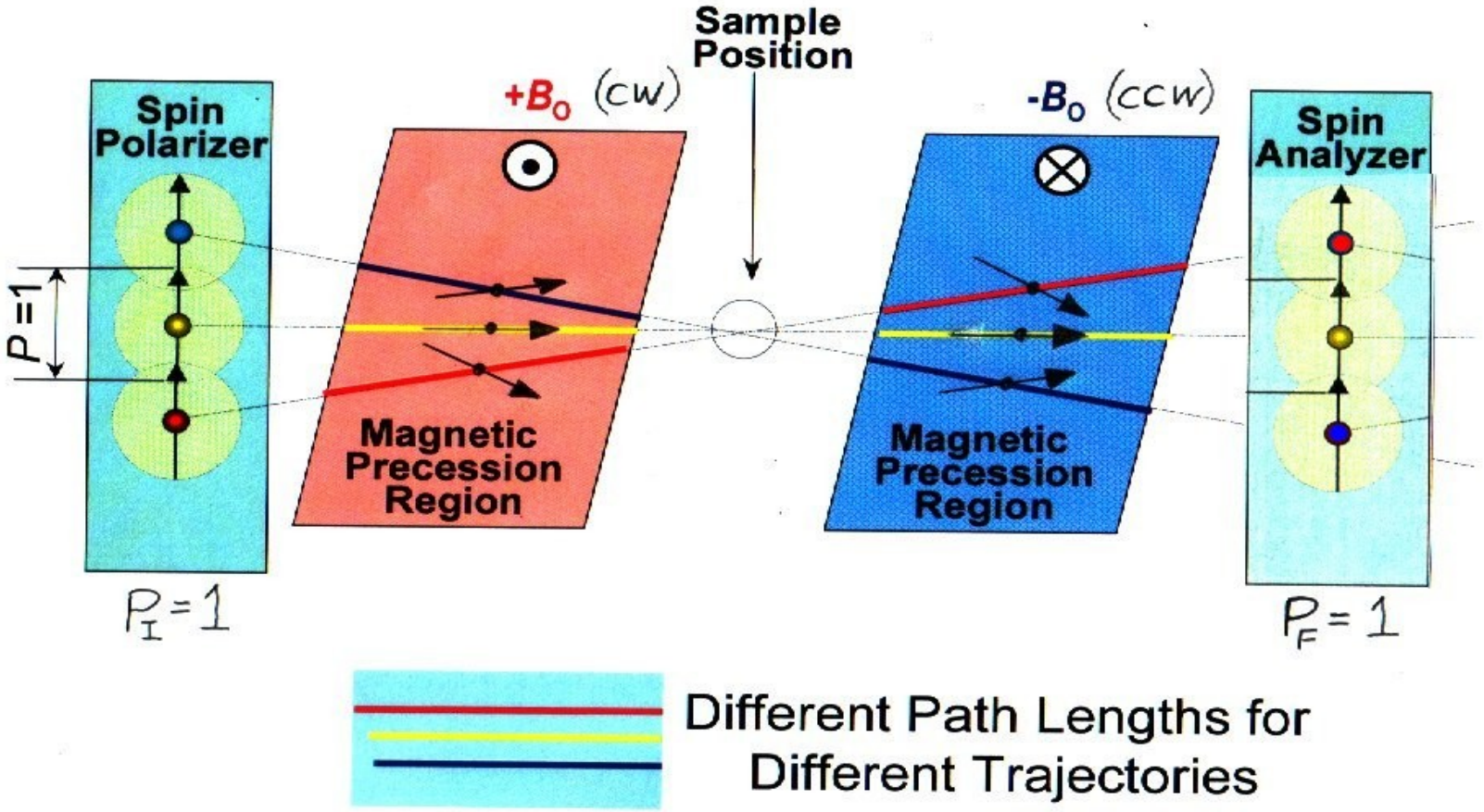

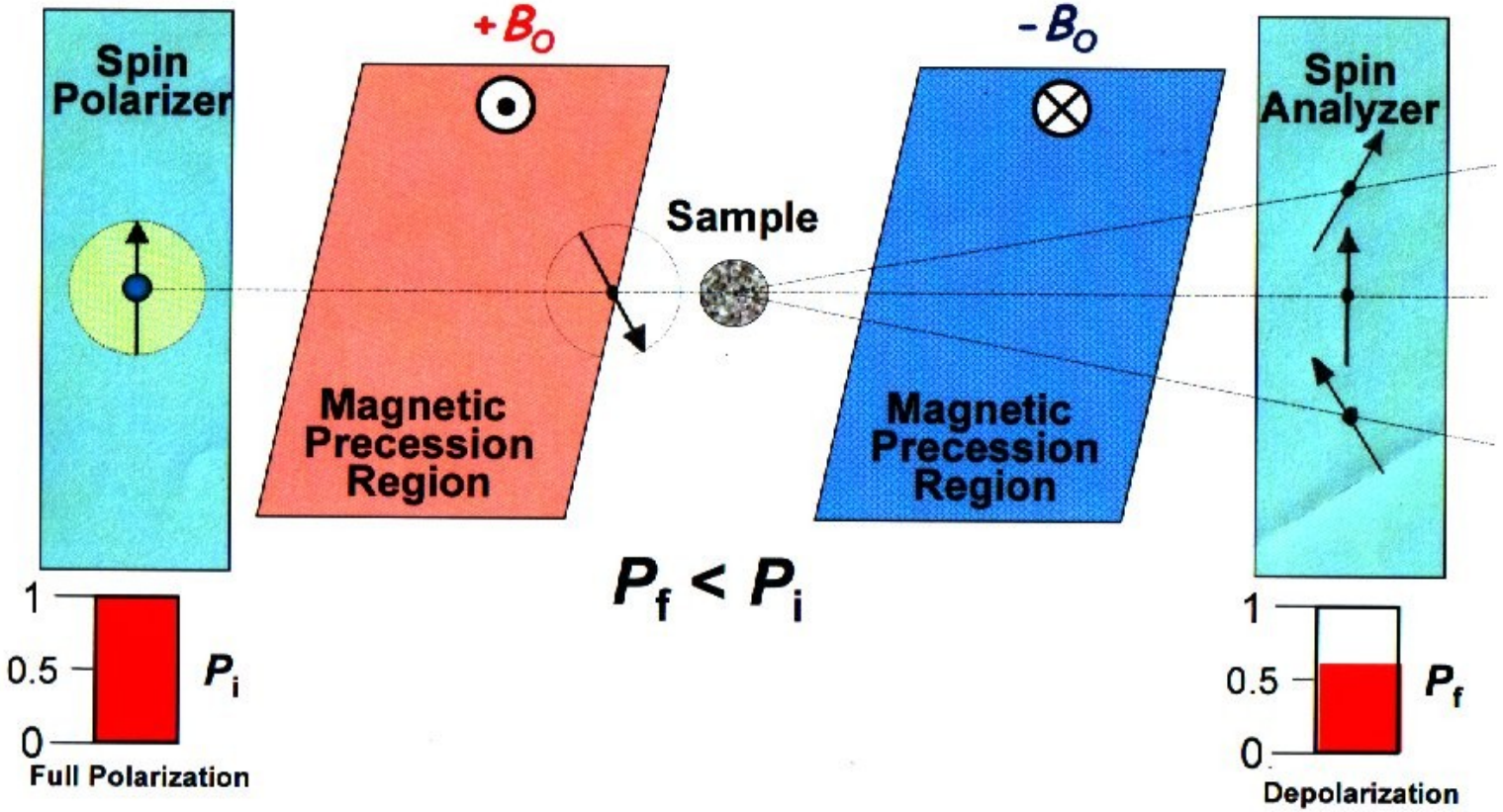
Spin Polarizer
+B_O
Magnetic Precession Region
Sample
-B_O
Magnetic Precession Region
Spin Analyzer
$P_f < P_i$
1
0.5
0
P_i
Full Polarization
1
0.5
0
P_f
Depolarization

NSE LABELLING OF ANGLE : PRECESSION FIELD GEOMETRY

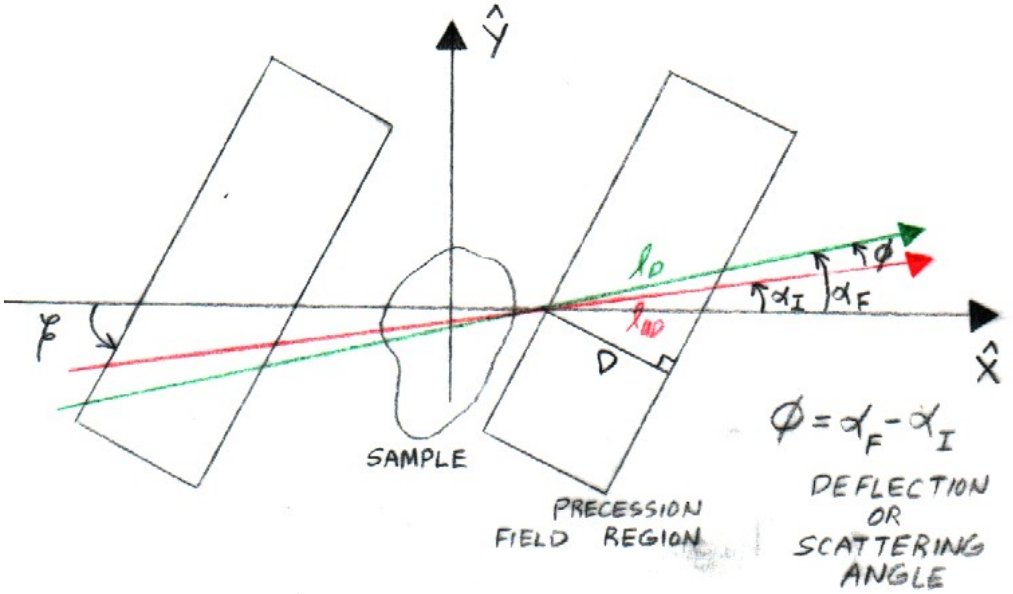

$$\ell_D \sin(\xi - \alpha_F) = D = \ell_{UD} \sin(\xi - \alpha_I)$$

PATH LENGTH DIFFERENCE $\Delta\ell = \ell_D - \ell_{UD}$

$$\Delta\ell = D\left[\frac{1}{\sin(\xi - \alpha_F)} - \frac{1}{\sin(\xi - \alpha_I)}\right]$$

AT SUFFICIENTLY SMALL ANGLES

$$\Delta\ell \simeq D\left(\frac{\cos\xi}{\sin^2\xi}\right)$$

DIFFRACTION FROM GRATING STRUCTURE ALONG Y-DIRECTION (IN PLANE)

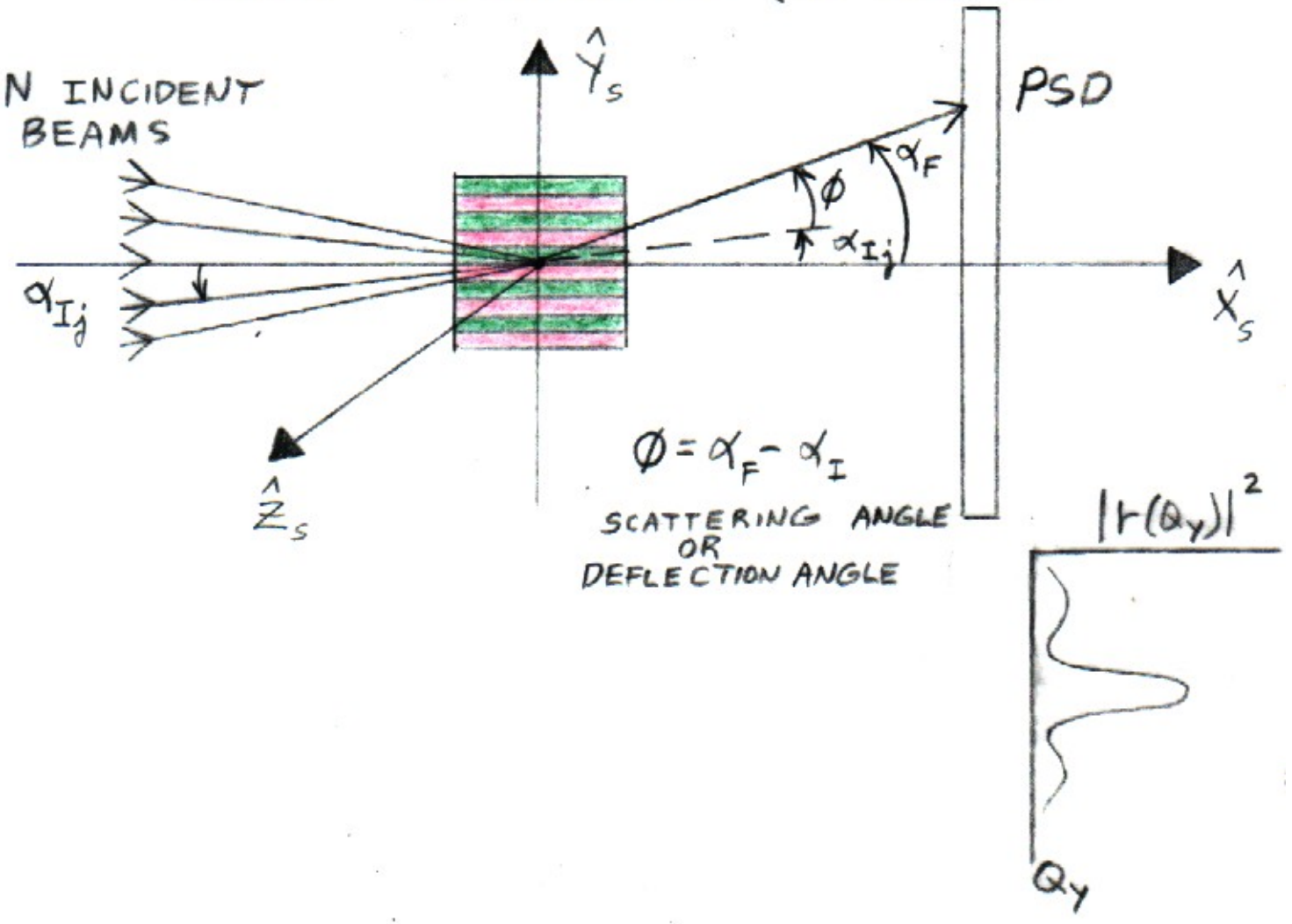

$|r|^2 \equiv$ REFLECTED INTENSITY / INCIDENT INTENSITY

J. Major et al., Physica B 336 (2003) 8-15

$$Q_y \simeq k(\alpha_F - \alpha_I) \equiv k\phi$$

$$|r_{BA}(Q_y)|^2 \propto \left| \int \rho(y) e^{iQ_y y} dy \right|^2$$

$$P_x(\delta^{SE}) = \int |r(\phi)|^2 \cos(k\phi\delta^{SE}) d\phi$$

WHERE $\underbrace{\delta^{SE}}_{\text{SPIN ECHO "LENGTH"}} = \underbrace{\left[\frac{m_n \gamma_n \lambda^2}{2\pi h}\right]}_{\text{CONSTANT}} \left(\frac{B D}{\sin\xi} \frac{\cos\xi}{\sin\xi}\right)$

ξ: PRECESSION FIELD TILT ANGLE

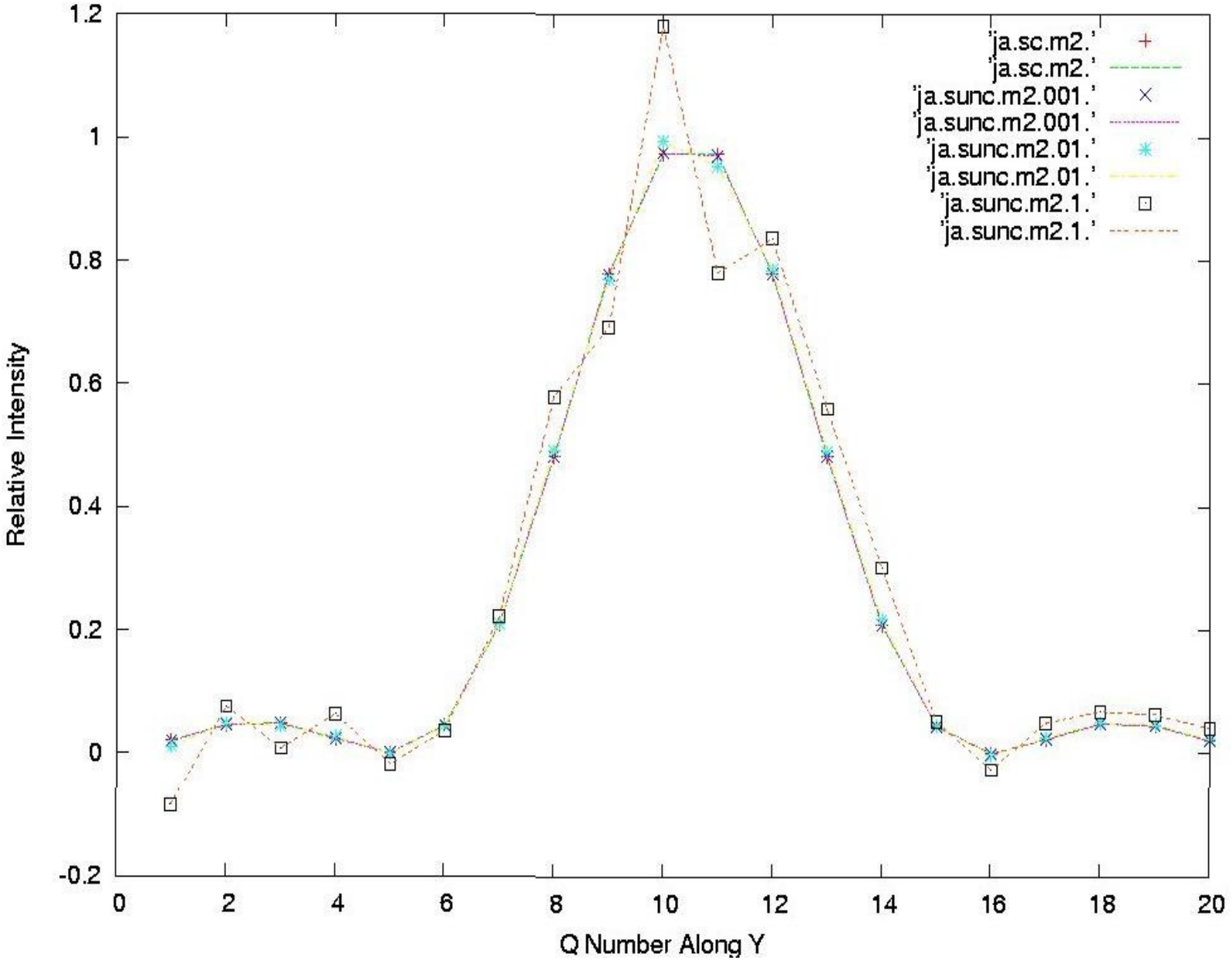

Comparison of inverted grating diffraction pattern to model where modulation of the beam was performed according to the spin-echo labeling method (blue asterisk symbols correspond to model and squares to calculated inversion).

Compact magnetic films replace precession coils.

Spin Echo Spectrometer
on NG5 at the NCNR

Spin Tagging Demonstration[1]
on EVA at the ILL, France

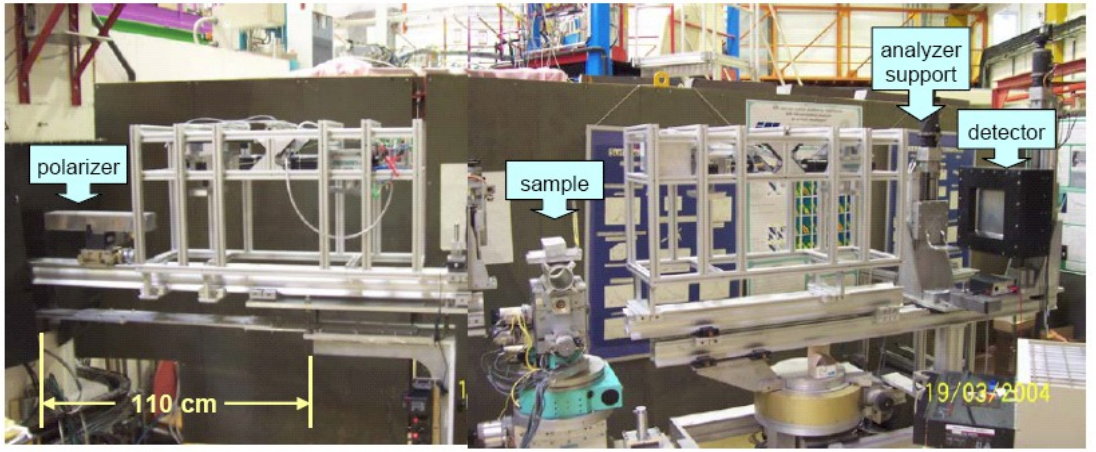

[1]J. Major, H. Dosch, G.P. Felcher, *et al*., Physica B (2003).
Also, M. Th. Rekveldt, *et al.,* Rev. Sci. Instr. (2005).
And R. Pynn, M.R. Fitzsimmons, *et al*., Rev. Sci. Instr. (2005).

“Polarized Neutron Reflectometry”, C.F.Majkrzak, K.V.O'Donovan, and N.F.Berk, Chapter 9 in *Neutron Scattering from Magnetic Materials*, Edited by T.Chatterji, (Elsevier, Amsterdam, 2006) p.397-471.

Polarized Neutrons, W. Gavin Williams, (Clarendon Press, Oxford, 1988)

www.ncnr.nist.gov -- variety of references and articles on the subject of polarized neutron scattering.

Zero-Field Neutron Polarimetry References

P.J.Brown, V.Nunez, F.Tasset, J.B.Forsyth and P.Radhakrishna
J.Phys.:Condens.Matter **2** (1990) 9409
Determination of the magnetic structure of Mn_3Sn using generalized neutron polarization analysis

V.Nunez, P.J.Brown, J.B.Forsyth and F.Tasset
Physica B **174** (1991) 60
Zero-field neutron polarimetry

P.J.Brown, T.Chattopadhyay, J.B.Forsyth, V.Nunez and F.Tasset
J.Phys.:Condens. Matter **3** (1991)
Antiferromagnetism in CuO studied by neutron polarimetry